Physica D 435 (2022) 133274

Contents lists available at ScienceDirect

Physica D

journal homepage: www.elsevier.com/locate/physd

N-double poles solutions for nonlocal Hirota equation with nonzero boundary conditions using Riemann–Hilbert method and PINN algorithm

Wei-Qi Peng [a], Yong Chen [a,b,*]

[a] School of Mathematical Sciences, Shanghai Key Laboratory of PMMP, East China Normal University, Shanghai, 200241, China
[b] College of Mathematics and Systems Science, Shandong University of Science and Technology, Qingdao, 266590, China

ARTICLE INFO

Article history:
Received 5 January 2022
Received in revised form 18 March 2022
Accepted 24 March 2022
Available online 9 April 2022
Communicated by Jingsong He

Keywords:
Nonlocal Hirota equation
Riemann–Hilbert method
Nonzero boundary conditions
Simple/double poles solutions
Physics-informed neural networks

ABSTRACT

In this paper, we systematically investigate the nonlocal Hirota equation with nonzero boundary conditions via Riemann–Hilbert method and multi-layer physics-informed neural networks algorithm. Starting from the Lax pair of nonzero nonlocal Hirota equation, we first give out the Jost function, scattering matrix, their symmetry and asymptotic behavior. Then, the Riemann–Hilbert problem with nonzero boundary conditions are constructed and the precise formulae of N-double poles solutions and N-simple poles solutions are written by determinants. Different from the local Hirota equation, the symmetry of scattering data for nonlocal Hirota equation is completely different, which results in disparate discrete spectral distribution. In particular, it could be more complicated and difficult to obtain the symmetry of scattering data under the circumstance of double poles. Besides, we also analyze the asymptotic state of one-double poles solution as $t \to \infty$. Whereafter, the multi-layer physics-informed neural networks algorithm is applied to research the data-driven soliton solutions of the nonzero nonlocal Hirota equation by using the training data obtained from the Riemann–Hilbert method. Most strikingly, the integrable nonlocal equation is firstly solved via multi-layer physics-informed neural networks algorithm. As we all know, the nonlocal equations contain the $\mathcal{PT}$ symmetry $\mathcal{P}: x \to -x$, or $\mathcal{T}: t \to -t$, which are different with local ones. Adding the nonlocal term into the neural network, we can successfully solve the integrable nonlocal Hirota equation by multi-layer physics-informed neural networks algorithm. The numerical results show that the algorithm can recover the data-driven soliton solutions of the integrable nonlocal equation well. Noteworthily, the inverse problems of the integrable nonlocal equation are discussed for the first time through applying the physics-informed neural networks algorithm to discover the parameters of the equation in terms of its soliton solution.

1. Introduction

It is well-known that nonlinear partial differential equation (PDE) plays a prominent role in the subjects of mathematical physics, such as fluid mechanics, nonlinear optics, ocean communication, etc. In the history of soliton theory, finding exact solutions of integrable PDE is still a crucial issue. During the past several decades, in order to solve nonlinear evolution equations, more and more methods and techniques have been presented including inverse scattering transformation (IST) [1], Hirota bilinear method [2], Darboux transformation (DT) [3], etc. Among them, IST method is one of the most powerful techniques to analyze the Cauchy problems of integrable nonlinear evolution equations. In 1967, Gardner et al. came up with this method first to handle the KdV equation with initial value problem [4]. The critical point of classic IST method is to solve the Gel'fand–Levitan–Marchenko (GLM) integral equations. Later on, Zakharov et al. developed a Riemann–Hilbert (RH) formulation which simplifies the IST method [5]. After that, the RH formulation has been constantly applied to numerous integrable equations with zero boundary conditions (ZBCs), such as coupled nonlinear Schrödinger (NLS) equation, derivative Schrödinger equation, Sasa–Satsuma equation, and so on [6–13]. Recently, the RH method was also applied to construct the soliton solutions [14–18] and the rogue waves [19–21] for the integrable equations with nonzero boundary conditions (NZBCs). Specially, through using the Laurent's series and generalization of the residue theorem, multiple high-order poles solutions have been studied for the NLS equation under ZBCs [22] and the focusing NLS under NZBCs [23]. Also, the $\bar{\partial}$-dressing method is developed to study the three-component

* Corresponding author at: School of Mathematical Sciences, Shanghai Key Laboratory of PMMP, East China Normal University, Shanghai, 200241, China.
E-mail address: ychen@sei.ecnu.edu.cn (Y. Chen).

https://doi.org/10.1016/j.physd.2022.133274
0167-2789/

coupled Hirota equations [24]. Moreover, the RH method has been employed to perform asymptotic analysis for some integrable equations, including the generalized derivative NLS [25], coupled NLS equation [26], the focusing NLS equation [27], and so on.

With the rapid development of machine learning methods, deep learning has become a powerful tool for solving PDE. Recently, a new neural network (NN), named physics-informed neural networks (PINN), was recently proposed, which can be used to accomplish the high-dimensional network tasks with fewer data sets [28]. Besides, it is verified that PINN is very effective for solving and inverting equations controlled by mathematical physical systems. Later on, PINN method was used to generate data-driven solutions and reveal the dynamic behavior of nonlinear PDE with physical constraints, which has attracted extensive attention and become a hot research topic. Very recently, in terms of PINN method, Chen group constructed data-driven soliton solution, high-order breather wave, rogue wave, rogue periodic wave for several types of nonlinear evolution equations including KdV equation, KN equation, Chen–Lee–Liu equation, etc. [29–31]. Particularly, based on conserved quantities, a two-stage PINN method was used to derive some data-driven localized wave solutions [32]. Besides, other scholars have also come up with some important results on data-driven solutions for the NLS equation and coupled NLS equation [33–36]. Thus it is natural to consider how to apply the PINN in the nonlocal integrable system. In this paper, we devote to construct a new PINN for solving the nonlocal integrable system via adding the nonlocal term into the NN, and the data-driven solution will be simulated through using the new PINN.

The parity-time ($\mathcal{PT}$) symmetry, first proposed in quantum mechanics by Bender and his coworkers, plays an important role in characterizing the wave propagation for the NLS equation in mechanical systems, optical fibers and magnetism [37–39]. Up to now, the research of $\mathcal{PT}$ system has made great progress in both theory and application [40–42]. For instance, Ablowitz and Musslimani first introduced the $\mathcal{PT}$ symmetry to the well-known AKNS system by raising a nonlocal (also named reverse-space) NLS equation [43]

$$\begin{aligned} &u_t(x,t) - iu_{xx}(x,t) \pm 2iQ(x,t)\,u(x,t) = 0,\\ &Q(x,t) = u(x,t)\,u^*(-x,t), \end{aligned} \tag{1.1}$$

which includes the $\mathcal{PT}$ symmetric potential $Q(x,t)$ and satisfies the $\mathcal{PT}$ symmetry restriction $Q(x,t) = Q^*(-x,t)$. The $*$ represents complex conjugate, and $Q(x,t)$ denotes electric field envelope and complex refractive index distribution of beam. Since then, Fokas extended the nonlocal NLS equation to a higher dimensional form [44]. Moreover, other nonlocal integrable equations were also investigated, such as nonlocal Davey–Stewartson equations, nonlocal modified KdV equation, nonlocal sine–Gordon equation, nonlocal derivative NLS equation, etc. [45–51]. It is worth mentioning that several nonlocal integrable equations with NZBCs have been researched through developing the IST [52–55]. After that, soliton solutions and high-order pole solutions for both focusing and defocusing nonlocal mKdV equations with NZBCs at infinity have been presented by a systematical inverse scattering transform [56,57].

Recently, starting with

$$\begin{aligned} &iq_t + \kappa\left[q_{xx} - 2q^2r\right] + i\beta\left[q_{xxx} - 6qrq_x\right] = 0,\\ &ir_t - \kappa\left[r_{xx} - 2qr^2\right] + i\beta\left[r_{xxx} - 6qrr_x\right] = 0, \end{aligned} \tag{1.2}$$

an integrable nonlocal (also named reverse-space–time) Hirota equation

$$q_t + \delta\left[q_{xx} - 2q^2q^*(-x,-t)\right] + \beta\left[q_{xxx} - 6qq^*(-x,-t)q_x\right] = 0, \tag{1.3}$$

was reduced in Ref. [58] for $r = q^*(-x,-t), \kappa = i\delta$. Of which $\delta, \beta \in \mathbb{R}$ are arbitrary parameters. Eq. (1.3) changes into the reverse-space–time nonlocal complex mKdV equation at the case of $\delta = 0, \beta = 1$. Besides, for the $\mathcal{PT}$ symmetric case $q^*(-x,-t) = q(x,t)$, Eq. (1.3) becomes the usual Hirota equation. The explicit multi-soliton solutions were generated for Eq. (1.3) by employing Hirota's direct method as well as Darboux–Crum transformations [58]. In what follows, we would like to write out its Lax pair firstly based on the early results [58], given by

$$\begin{aligned} &\Psi_x = U\Psi, \qquad U \equiv \begin{pmatrix} -i\lambda & q(x,t) \\ q^*(-x,-t) & i\lambda \end{pmatrix},\\ &\Psi_t = V\Psi, \qquad V \equiv \begin{pmatrix} \tilde{A}(x,t) & \tilde{B}(x,t) \\ \tilde{C}(x,t) & -\tilde{A}(x,t) \end{pmatrix},\\ &\tilde{A} = \delta qq^*(-x,-t) + 2\delta\lambda^2 + \beta\left[q^*(-x,-t)q_x - qq_x^*(-x,-t)\right.\\ &\quad \left.-4i\lambda^3 - 2i\lambda qq^*(-x,-t)\right],\\ &\tilde{B} = -\delta q_x + 2i\delta\lambda q + \beta\left[2q^2q^*(-x,-t) - q_{xx} + 2i\lambda q_x + 4\lambda^2 q\right],\\ &\tilde{C} = \delta q_x^*(-x,-t) + 2i\delta\lambda q^*(-x,-t)\\ &+\beta\left[2qq^*(-x,-t)^2 - q_{xx}^*(-x,-t) - 2i\lambda q_x^*(-x,-t)\right.\\ &\quad \left.+4\lambda^2 q^*(-x,-t)\right]. \end{aligned} \tag{1.4}$$

To the best of our knowledge, although some people have studied the nonlocal Hirota equation with ZBCs [59–61], the studies of the nonlocal Hirota equation (1.3) with NZBCs have been rarely reported via using RH method, because the RH method with NZBCs is more complicated than one with ZBCs. In what follows, we would systematically consider the matrix RH problem for the nonlocal Hirota equation (1.3) with following NZBCs at infinity

$$\lim_{x\to\pm\infty} q(x,t) = q_\pm e^{2\delta q_0^2 t}, \tag{1.5}$$

where $|q_\pm| = q_0 > 0$, and $q_+ = q_-$ are constant. Different from previous work about the usual Hirota equation, the nonlocal Hirota equation involves different symmetry reductions and disparate discrete spectra distribution. Especially, for the case of double poles, symmetry could be more complicated. It is worth mentioning that the asymptotic state of one-double poles solution is also given out as $t \to \infty$. Furthermore, we also find that PINN deep learning for solving nonlocal integrable equation has not been researched so far. Therefore, in this paper, we also commit to propose a scheme to solve integrable nonlocal equation in terms of PINN method. As an example, we choose the integrable nonzero nonlocal Hirota equation to highlight the ability of our strategy to handle the integrable nonlocal equation, and successfully predict the data-driven soliton solution of the nonzero nonlocal Hirota equation. On the other hand, we also discuss the data-driven parameter discovery for the nonzero nonlocal Hirota equation.

The outline of this paper is organized as follows: In Section 2, we carry out the spectral analysis for nonlocal Hirota equation under NZBCs, and derive the corresponding Lax pair, Jost solutions, scattering matrix and their symmetry reductions. In Sections 3 and 4, through analyzing the inverse scattering problem for nonlocal Hirota equation under NZBCs, we establish the RH problem for the nonlocal Hirota equation under NZBCs and obtain the explicit N-simple poles solution and N-double poles solution for the reflectionless coefficients under NZBCs. In Section 5, the data-driven soliton solutions and data-driven parameter discovery for the nonlocal Hirota equation are researched via PINN method. Finally, some summaries are given in the last section.

2. Spectral analysis for nonlocal hirota equation under NZBCs

2.1. Lax pair and jost solutions

In order to facilitate the later calculation, we deal with Lax pair (1.4) with the boundary condition (1.5) at the beginning. Let us make an appropriate transformation

$$q \to q e^{2\delta q_0^2 t}, \qquad \Psi \to e^{\delta q_0^2 t \sigma_3}\Psi, \tag{2.1}$$

where σ_3 is one of the following Pauli matrices

$$\sigma_1 = \begin{pmatrix} 0 & 1 \\ 1 & 0 \end{pmatrix}, \quad \sigma_2 = \begin{pmatrix} 0 & -i \\ i & 0 \end{pmatrix}, \quad \sigma_3 = \begin{pmatrix} 1 & 0 \\ 0 & -1 \end{pmatrix}. \tag{2.2}$$

Then, the nonlocal Hirota equation (1.3) changes into

$$q_t + \delta\left[q_{xx} - 2q^2 q^*(-x,-t) + 2q_0^2 q\right] + \beta\left[q_{xxx} - 6qq^*(-x,-t)q_x\right] = 0, \tag{2.3}$$

with following boundary

$$\lim_{x\to\pm\infty} q(x,t) = q_\pm, \tag{2.4}$$

which admits the Lax pair

$$\begin{aligned} &\Psi_x = U\Psi, \qquad U \equiv \begin{pmatrix} -i\lambda & q(x,t) \\ q^*(-x,-t) & i\lambda \end{pmatrix}, \\ &\Psi_t = V\Psi, \qquad V \equiv \begin{pmatrix} \tilde{A}(x,t) - \delta q_0^2 & \tilde{B}(x,t) \\ \tilde{C}(x,t) & -\tilde{A}(x,t) + \delta q_0^2 \end{pmatrix}. \end{aligned} \tag{2.5}$$

As $x \to \pm\infty$, the Lax pair (2.5) under the boundary (2.4) becomes

$$\begin{aligned} &\Psi_x = U_\pm\Psi = (-i\lambda\sigma_3 + Q_\pm)\Psi, \\ &\Psi_t = V_\pm\Psi = \left[2i\delta\lambda + \beta(4\lambda^2 + 2q_0^2)\right]U_\pm\Psi, \end{aligned} \tag{2.6}$$

where

$$Q_\pm = \begin{pmatrix} 0 & q_\pm \\ q_\mp^* & 0 \end{pmatrix}. \tag{2.7}$$

The system (2.6) can be solved by

$$\Psi_\pm^{bg}(x,t,\lambda) = \begin{cases} Y_\pm(\lambda)e^{-i\theta(x,t,\lambda)\sigma_3}, & \lambda \neq \pm q_0 \\ I + \left(x + \left(2i\delta\lambda + \beta(4\lambda^2 + 2q_0^2)\right)t\right)U_\pm(\lambda), & \lambda = \pm q_0, \end{cases} \tag{2.8}$$

where

$$\begin{aligned} &Y_\pm = \begin{pmatrix} 1 & -\frac{iq_\pm}{\lambda+k} \\ \frac{iq_\mp^*}{\lambda+k} & 1 \end{pmatrix}, \\ &\theta(x,t,k) = k[x + \left(2i\delta\lambda + \beta(4\lambda^2 + 2q_0^2)\right)t], \quad k^2 = \lambda^2 - q_0^2. \end{aligned} \tag{2.9}$$

In order to analyze the scattering problem on a standard z-plane instead of the two-sheeted Riemann surface, we introduce a uniformization variable $z = k + \lambda$, given by

$$k = \frac{1}{2}(z - \frac{q_0^2}{z}), \qquad \lambda = \frac{1}{2}(z + \frac{q_0^2}{z}). \tag{2.10}$$

Setting D_+, D_- and Σ on z-plane as $D_\pm = \{z \in \mathbb{C} | \mathrm{Im} z \gtrless 0\}$, $\Sigma = \mathbb{R}$, the Jost solutions $\Psi_\pm(x,t,z)$ are defined by

$$\Psi_\pm(x,t,z) = Y_\pm e^{-i\theta(x,t,z)\sigma_3} + o(1), \quad z \in \Sigma, \quad \text{as} \quad x \to \pm\infty. \tag{2.11}$$

Using the variable transformation

$$\mu_\pm(x,t,z) = \Psi_\pm(x,t,z)e^{i\theta(x,t,z)\sigma_3}, \tag{2.12}$$

we get the modified Jost solutions $\mu_\pm(x,t,z) \to Y_\pm(z)$ as $x \to \pm\infty$, which satisfy the following Volterra integral equations

$$\begin{aligned} &\mu_\pm(x,t,z) \\ &= \begin{cases} Y_\pm + \int_{\pm\infty}^x Y_\pm e^{-ik(x-y)\hat{\sigma}_3}\left[Y_\pm^{-1}\Delta U_\pm(y,t)\mu_\pm(y,t,z)\right]dy, & z \neq \pm q_0, \\ Y_\pm + \int_{\pm\infty}^x \left[I + (x-y)U_\pm(z)\right]\Delta U_\pm(y,t)\mu_\pm(y,t,z)dy, & z = \pm q_0, \end{cases} \end{aligned} \tag{2.13}$$

where $\Delta U_\pm = U - U_\pm$.

Proposition 2.1. *Assume $q - q_\pm \in L^1(\mathbb{R}^\pm)$, then $\mu_\pm(x,t,z)$ defined in Eq. (2.12) uniquely solve the Volterra integral Eq. (2.13) in $\Sigma_0 = \Sigma \setminus \{\pm q_0\}$, and $\mu_\pm(x,t,z)$ yield:*

- *$\mu_{-1}(x,t,z)$ and $\mu_{+2}(x,t,z)$ is analytical in D_+ and continuous in $D_+ \cup \Sigma_0$,*
- *$\mu_{+1}(x,t,z)$ and $\mu_{-2}(x,t,z)$ is analytical in D_- and continuous in $D_- \cup \Sigma_0$,*
- *$\mu_\pm(x,t,z) \to I$ as $z \to \infty$,*
- *$\mu_\pm(x,t,z) \to -\frac{i}{z}\sigma_3 Q_\pm$ as $z \to 0$,*
- *$\det \mu_\pm(x,t,z) = \det Y_\pm = \gamma = 1 - \frac{q_0^2}{z^2}, \quad x,t \in \mathbb{R}, \quad z \in \Sigma_0.$*

Since the Jost solutions $\Psi_\pm(x,t,z)$ are the simultaneous solutions of Lax pair (2.5), we can establish the linear relation by a scattering matrix $S(z) = (s_{ij}(z))_{2\times 2}$, given by

$$\Psi_+(x,t,z) = \Psi_-(x,t,z)S(z), \quad z \in \Sigma_0. \tag{2.14}$$

We can write the scattering coefficients into the form of Wronskians determinant

$$\begin{aligned} &s_{11}(z) = \frac{Wr(\Psi_{+,1}, \Psi_{-,2})}{\gamma(z)}, \quad s_{12}(z) = \frac{Wr(\Psi_{+,2}, \Psi_{-,2})}{\gamma(z)}, \\ &s_{21}(z) = \frac{Wr(\Psi_{-,1}, \Psi_{+,1})}{\gamma(z)}, \quad s_{22}(z) = \frac{Wr(\Psi_{-,1}, \Psi_{+,2})}{\gamma(z)}. \end{aligned} \tag{2.15}$$

Proposition 2.2. *Suppose $q - q_\pm \in L^1(\mathbb{R}^\pm)$, then the scattering matrix $S(z)$ has the following characteristics:*

- *$\det S(z) = 1$ for $z \in \Sigma_0$,*
- *$s_{22}(z)$ is analytical in D_+ and continuous in $D_+ \cup \Sigma_0$,*
- *$s_{11}(z)$ is analytical in D_- and continuous in $D_- \cup \Sigma_0$,*
- *$S(x,t,z) \to I$ as $z \to \infty$,*
- *$S(x,t,z) \to I$ as $z \to 0$.*

2.2. Symmetry reductions

In this subsection, according to the reduction conditions of the Lax pair on the complex z-plane, the symmetries of the Jost solutions $\Psi(x,t,z)$ and scattering matrix $S(z)$ are studied for the nonlocal Hirota equation with NZBCs. The details are as follows:

Proposition 2.3. *The $X(x,t,z)$ and $T(x,t,z)$ in the Lax pair (2.5) meet the following reduction conditions on z-plane:*

- *The first symmetry reduction*

$$\begin{aligned} &U(x,t,z) = -\sigma_2 U(-x,-t,-z^*)^*\sigma_2, \\ &V(x,t,z) = -\sigma_2 V(-x,-t,-z^*)^*\sigma_2. \end{aligned} \tag{2.16}$$

- *The second symmetry reduction*

$$U(x,t,z) = U(x,t,\frac{q_0^2}{z}), \qquad V(x,t,z) = V(x,t,\frac{q_0^2}{z}). \tag{2.17}$$

Proposition 2.4. *The Jost solutions $\Psi(x,t,z)$ and scattering matrix $S(z)$ possess the following reduction conditions on z-plane:*

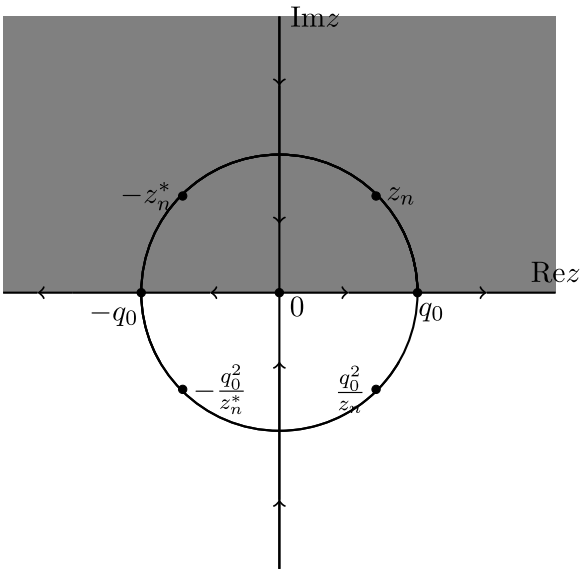

Fig. 1. Distribution of the discrete spectrum and jumping curves for the RH problem on complex z-plane, Region $D_+ = \{z \in \mathbb{C}|\mathrm{Im}z > 0\}$ (gray region), region $D_- = \{z \in \mathbb{C}|\mathrm{Im}z < 0\}$ (white region).

- *The first symmetry reduction*

$$\Psi_\pm(x,t,z) = \sigma_2\Psi_\mp(-x,-t,-z^*)^*\sigma_2, \qquad S(z) = \sigma_2 S^*(-z^*)^{-1}\sigma_2. \tag{2.18}$$

- *The second symmetry reduction*

$$\Psi_\pm(x,t,z) = -\frac{i}{z}\Psi_\pm(x,t,\frac{q_0^2}{z})\sigma_3 Q_\pm, \qquad S(z) = Q_-^{-1}\sigma_3 S(\frac{q_0^2}{z})\sigma_3 Q_+. \tag{2.19}$$

2.3. Discrete spectrum with simple poles

In this subsection, assuming that $s_{22}(z)$ has N simple zeros z_n $(n = 1,2,\ldots,N)$ in $D_+ \cap \{z \in \mathbb{C} : \mathrm{Re}z > 0\}$, then we have $s_{22}(z_0) = 0$ and $s'_{22}(z_0) \neq 0$ in the situations of z_0 being the simple zero of $s_{22}(z)$. In terms of the symmetries of the scattering matrix, the corresponding discrete spectrum is summarized into (see Fig. 1)

$$\Upsilon = \left\{z_n, -z_n^*, \frac{q_0^2}{z_n}, -\frac{q_0^2}{z_n^*}\right\}_{n=1}^N, \tag{2.20}$$

where z_n satisfies that $|z_n| = q_0$.

Considering $s_{22}(z_0) = 0$ $(z_0 \in \Upsilon \cap D_+)$, it is not hard to find that $\Psi_{-1}(x,t,z_0)$ and $\Psi_{+2}(x,t,z_0)$ are linearly dependent. Homoplastically, $\Psi_{+1}(x,t,z_0)$ and $\Psi_{-2}(x,t,z_0)$ are linearly dependent because of $s_{11}(z_0) = 0$ $(z_0 \in \Upsilon \cap D_-)$. Then, one has

$$\begin{aligned}&\Psi_{+2}(x,t,z_0) = b[z_0]\Psi_{-1}(x,t,z_0), \quad z_0 \in \Upsilon \cap D_+,\\ &\Psi_{+1}(x,t,z_0) = b[z_0]\Psi_{-2}(x,t,z_0), \quad z_0 \in \Upsilon \cap D_-,\end{aligned} \tag{2.21}$$

where $b[z_0]$ is a undetermined parameter. Therefore, we arrive at

$$\begin{aligned}&\mathop{\mathrm{Res}}_{z=z_0}\left[\frac{\Psi_{+2}(x,t;z)}{s_{22}(z)}\right] = A[z_0]\Psi_{-1}(x,t;z_0), \quad z_0 \in \Upsilon \cap D_+,\\ &\mathop{\mathrm{Res}}_{z=z_0}\left[\frac{\Psi_{+1}(x,t;z)}{s_{11}(z)}\right] = A[z_0]\Psi_{-2}(x,t;z_0), \quad z_0 \in \Upsilon \cap D_-,\end{aligned} \tag{2.22}$$

where

$$A[z_0] = \begin{cases} \frac{b[z_0]}{s'_{22}(z_0)}, & z_0 \in \Upsilon \cap D_+,\\ \frac{b[z_0]}{s'_{11}(z_0)}, & z_0 \in \Upsilon \cap D_-.\end{cases} \tag{2.23}$$

Proposition 2.5. *Two relations for $b[z_0]$, $s'_{22}(z_0)$ and $s'_{11}(z_0)$ are got below:*

- *The first relation*

$$\begin{aligned}&b[z_0] = -\frac{1}{b[-z_0^*]^*}, \quad s'_{11}(z_0) = -s'_{11}(-z_0^*)^*,\\ &s'_{22}(z_0) = -s'_{22}(-z_0^*)^*.\end{aligned} \tag{2.24}$$

- *The second relation*

$$\begin{aligned}&b[z_0] = -\frac{q_+}{q_-^*}b[\frac{q_0^2}{z_0}], \quad s'_{22}(z_0) = -\frac{q_0^2}{z_0^2}s'_{11}(\frac{q_0^2}{z_0}), \quad z_0 \in D_+,\\ &b[z_0] = -\frac{q_+^*}{q_-}b[\frac{q_0^2}{z_0}], \quad s'_{11}(z_0) = -\frac{q_0^2}{z_0^2}s'_{22}(\frac{q_0^2}{z_0}), \quad z_0 \in D_-.\end{aligned} \tag{2.25}$$

3. Inverse scattering problem for nonlocal hirota equation under NZBCs: simple poles

3.1. The Riemann-Hilbert problem under NZBCs

In terms of the analyticity of Jost solutions $\mu_\pm(x,t,z)$ in Proposition 2.1, the following sectionally meromorphic matrices can be defined

$$M_-(x,t,z) = (\frac{\mu_{+1}}{s_{11}}, \mu_{-2}), \qquad M_+(x,t,z) = (\mu_{-1}, \frac{\mu_{+2}}{s_{22}}), \tag{3.1}$$

where $\pm$ represent analyticity in D_+ and D_-, respectively. Subsequently, a matrix RH problem is constructed:

Riemann–Hilbert Problem *$M(x,t,z)$ solves the following RHP:*

$$\begin{cases} M(x,t,z) \text{ is analytic in } \mathbb{C}\setminus\Sigma,\\ M_-(x,t,z) = M_+(x,t,z)(I - G(x,t,z)), \qquad z \in \Sigma,\\ M(x,t,z) \to I, \qquad z \to \infty,\\ M(x,t,z) \to -\frac{i}{z}\sigma_3 Q_-, \qquad z \to 0,\end{cases} \tag{3.2}$$

of which the jump matrix $G(x,t,z)$ is

$$G = \begin{pmatrix} \rho(z)\tilde{\rho}(z) & e^{-2i\theta(x,t,z)}\tilde{\rho}(z)\\ -e^{2i\theta(x,t,z)}\rho(z) & 0\end{pmatrix}, \tag{3.3}$$

where $\rho(z) = \frac{s_{21}(z)}{s_{11}(z)}$, $\tilde{\rho}(z) = \frac{s_{12}(z)}{s_{22}(z)}$. Let

$$M(x,t,z) = I + \frac{1}{z}M^{(1)}(x,t;z) + O(\frac{1}{z^2}), \qquad z \to \infty, \tag{3.4}$$

then the potential $q(x,t)$ of the nonlocal Hirota equation (2.3) with NZBCs is given by

$$q(x,t) = iM_{12}^{(1)}(x,t,z) = i\lim_{z\to\infty} zM_{12}(x,t,z). \tag{3.5}$$

As a matter of convenience, we take $\hat{\zeta}_n = \frac{q_0^2}{\zeta_n}$ and define

$$\zeta_n = \begin{cases} z_n, & n = 1,2,\ldots,N,\\ -z_{n-N}^*, & n = N+1, N+2,\ldots,2N.\end{cases} \tag{3.6}$$

Then the residue of $M(x,t,z)$ is

$$\begin{aligned}&\mathop{\mathrm{Res}}_{z=\zeta_n} M_+ = \left(0, A[\zeta_n]e^{-2i\theta(x,t,\zeta_n)}\mu_{-1}(x,t,\zeta_n)\right),\\ &\mathop{\mathrm{Res}}_{z=\hat{\zeta}_n} M_- = \left(A[\hat{\zeta}_n]e^{2i\theta(x,t;\hat{\zeta}_n)}\mu_{-2}(x,t,\hat{\zeta}_n), 0\right).\end{aligned} \tag{3.7}$$

Through subtracting out the residue and the asymptotic values as $z \to \infty, z \to 0$ from the original non-regular RHP, the following regular RHP can be obtained

$$M_- + \frac{i}{z}\sigma_3 Q_- - I - \sum_{n=1}^{2N}\left[\frac{\mathrm{Res}M_+}{z-\zeta_n} + \frac{\mathrm{Res}M_-}{z-\hat{\zeta}_n}\right] = M_+ + \frac{i}{z}\sigma_3 Q_- - I - \sum_{n=1}^{2N}\left[\frac{\mathrm{Res}M_+}{z-\zeta_n} + \frac{\mathrm{Res}M_-}{z-\hat{\zeta}_n}\right] - M_+ G, \tag{3.8}$$

which can be solved by the Plemelj's formulae, given by

$$M(x,t;z) = I - \frac{i}{z}\sigma_3 Q_- + \frac{1}{2\pi i}\int_\Sigma \frac{M_+(x,t;\zeta)G(x,t;\zeta)}{\zeta - z}d\zeta + \sum_{n=1}^{2N}\left[\frac{\mathrm{Res}M_+}{z-\zeta_n} + \frac{\mathrm{Res}M_-}{z-\hat{\zeta}_n}\right], \tag{3.9}$$

where

$$\frac{\mathrm{Res}M_+}{z-\zeta_n} + \frac{\mathrm{Res}M_-}{z-\hat{\zeta}_n} = \left(\hat{C}_n(z)\mu_{-2}(\hat{\zeta}_n), C_n(z)\mu_{-1}(\zeta_n)\right), \tag{3.10}$$

and

$$C_n(z) = \frac{A[\zeta_n]e^{-2i\theta(\zeta_n)}}{z-\zeta_n}, \quad \hat{C}_n(z) = \frac{A[\hat{\zeta}_n]e^{2i\theta(\hat{\zeta}_n)}}{z-\hat{\zeta}_n}. \tag{3.11}$$

Furthermore, according to (3.4), one has

$$M^{(1)}(x,t,z) = -\frac{1}{2\pi i}\int_\Sigma M_+(x,t;\zeta)G(x,t;\zeta)d\zeta - i\sigma_3 Q_- + \sum_{n=1}^{2N}\left(A[\hat{\zeta}_n]e^{2i\theta(\hat{\zeta}_n)}\mu_{-2}(\hat{\zeta}_n), A[\zeta_n]e^{-2i\theta(\zeta_n)}\mu_{-1}(\zeta_n)\right). \tag{3.12}$$

Therefore, the potential $q(x,t)$ with simple poles for the nonlocal Hirota equation with NZBCs is given by

$$q(x,t) = iM_{12}^{(1)} = q_- + i\sum_{n=1}^{2N}A[\zeta_n]e^{-2i\theta(\zeta_n)}\mu_{-11}(\zeta_n) - \frac{1}{2\pi}\int_\Sigma (M_+(x,t;\zeta)G(x,t;\zeta))_{12}d\zeta. \tag{3.13}$$

3.2. Trace formulae and theta condition

The scattering coefficients $s_{22}(z)$ and $s_{11}(z)$ respectively have simple zeros ζ_n and $\hat{\zeta}_n$, thus we can take

$$\beta^+(z) = s_{22}(z)\prod_{n=1}^{2N}\frac{z-\hat{\zeta}_n}{z-\zeta_n}, \quad \beta^-(z) = s_{11}(z)\prod_{n=1}^{2N}\frac{z-\zeta_n}{z-\hat{\zeta}_n}, \tag{3.14}$$

that means $\beta^+(z)$ is analytic and has no zeros in D_+, and $\beta^-(z)$ is analytic and has no zeros in D_-. Also, $\beta^\pm(z) \to o(1)$ as $z \to \infty$. According to the Plemelj's formulae, $\beta^\pm(z)$ can be written as

$$\log\beta^\pm(z) = \mp\frac{1}{2\pi i}\int_\Sigma \frac{\log(1-\rho\tilde{\rho})}{s-z}ds, \quad z \in D^\pm. \tag{3.15}$$

Using Eq. (3.14), we derive the following trace formulae

$$s_{22}(z) = \exp\left[-\frac{1}{2\pi i}\int_\Sigma \frac{\log(1-\rho\tilde{\rho})}{s-z}ds\right]\prod_{n=1}^{2N}\frac{z-\zeta_n}{z-\hat{\zeta}_n},$$
$$s_{11}(z) = \exp\left[\frac{1}{2\pi i}\int_\Sigma \frac{\log(1-\rho\tilde{\rho})}{s-z}ds\right]\prod_{n=1}^{2N}\frac{z-\hat{\zeta}_n}{z-\zeta_n}. \tag{3.16}$$

Let $z \to 0$ in the first formula of Eq. (3.16), one has

$$\exp\left[\frac{i}{2\pi}\int_\Sigma \frac{\log(1-\rho\tilde{\rho})}{s}ds\right]\prod_{n=1}^{N}\frac{|z_n|^4}{q_0^4} = 1. \tag{3.17}$$

In addition, taking the derivative of Eq. (3.16) with respect to z, we obtain $s'_{22}(\zeta_j)$ and $s'_{11}(\hat{\zeta}_j)$, given by

$$s'_{22}(\zeta_j) = \exp\left[-\frac{1}{2\pi i}\int_\Sigma \frac{\log(1-\rho\tilde{\rho})}{s-\zeta_j}ds\right]\frac{\prod_{m\neq j}(\zeta_j-\zeta_m)}{\prod_{m=1}^{2N}(\zeta_j-\hat{\zeta}_m)},$$
$$s'_{11}(\hat{\zeta}_j) = \exp\left[\frac{1}{2\pi i}\int_\Sigma \frac{\log(1-\rho\tilde{\rho})}{s-\hat{\zeta}_j}ds\right]\frac{\prod_{m\neq j}(\hat{\zeta}_j-\hat{\zeta}_m)}{\prod_{m=1}^{2N}(\hat{\zeta}_j-\zeta_m)}. \tag{3.18}$$

3.3. The simple poles soliton solution of nonlocal hirota equation under NZBCs

In the case of no reflection, i.e. $\rho(z) = \tilde{\rho}(z) = 0$, we can get the soliton solution. We first take the second column of Eq. (3.9)

$$\mu_{-2}(z) = \begin{pmatrix} -\frac{i}{z}q_- \\ 1 \end{pmatrix} + \sum_{n=1}^{2N}C_n(z)\mu_{-1}(\zeta_n). \tag{3.19}$$

In terms of the symmetric relation, we easily get

$$\mu_{-2}(z) = -\frac{iq_-}{z}\mu_{-1}(\frac{q_0^2}{z}). \tag{3.20}$$

Substituting Eq. (3.20) into Eq. (3.19), and setting $z = \hat{\zeta}_j, j = 1,2,\ldots,2N$, we generate a $2N$ linear system:

$$\sum_{n=1}^{2N}\left(C_n(\hat{\zeta}_j) + \frac{iq_-}{\hat{\zeta}_j}\delta_{j,n}\right)\mu_{-1}(\zeta_n) + \begin{pmatrix} -\frac{i}{\hat{\zeta}_j}u_- \\ 1 \end{pmatrix} = 0. \tag{3.21}$$

Theorem 3.1. *The precise formulae of N-simple poles solutions for the nonlocal Hirota equation (2.3) with NZBCs (2.4) is expressed as*

$$q(x,t) = q_- - i\frac{\det\begin{pmatrix}\mathcal{H} & \varphi \\ \chi^T & 0\end{pmatrix}}{\det(\mathcal{H})}. \tag{3.22}$$

Proof. From Eq. (3.21), it is not hard to derive a $2N$ linear system with respect to $\mu_{-11}(\zeta_n)$

$$\sum_{n=1}^{2N}\left(C_n(\hat{\zeta}_j) + \frac{iq_-}{\hat{\zeta}_j}\delta_{j,n}\right)\mu_{-11}(\zeta_n) = \frac{iq_-}{\hat{\zeta}_j}, \quad j = 1,2,\ldots,2N. \tag{3.23}$$

The linear system can be rewritten into a matrix form:

$$\mathcal{H}\alpha = \varphi, \tag{3.24}$$

where $\mathcal{H} = (h_{jn})_{2N\times 2N}$, $\alpha = (\alpha_n)_{2N\times 1}$, $\varphi = (\varphi_j)_{2N\times 1}$ with

$$h_{jn} = C_n(\hat{\zeta}_j) + \frac{iq_-}{\hat{\zeta}_j}\delta_{j,n}, \quad \alpha_n = \mu_{-11}(\zeta_n), \quad \varphi_j = \frac{iq_-}{\hat{\zeta}_j}. \tag{3.25}$$

In the case of reflectionless potential, Eq. (3.13) is rewritten as

$$q = q_- + i\chi^T\alpha, \tag{3.26}$$

where $\chi = (\chi_n)_{2N\times 1}$ with $\chi_n = A[\zeta_n]e^{-2i\theta(\zeta_n)}$. Combining Eq. (3.24), the expression of the soliton solution is presented finally. □

As an example, through choosing some appropriate parameters, we discuss the dynamical behaviors for simple poles solution

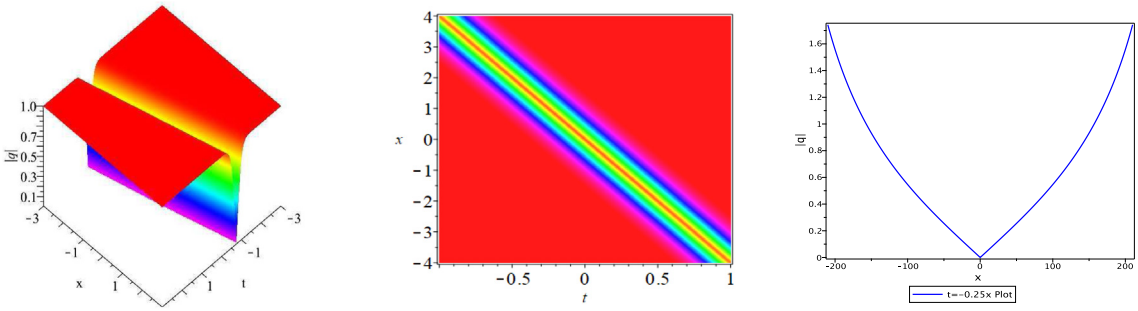

Fig. 2. One-simple pole solution for Eq. (2.3) with the parameters: $b_1 = 1, q_0 = 1, \vartheta_1 = \frac{\pi}{4}, \theta_- = 0, \delta = \frac{1}{100}, \beta = 1$. (**a**) Three dimensional plot; (**b**) The density plot; (**c**) The peak of wave along the line $t = -0.25x$ (blue).

in the case of $N = 1$ and $N = 2$, respectively. It is worth mentioning that the discrete spectrum cannot to be pure imaginary number, which is verified from Proposition 2.5.

Case 1: $N = 1$

Let $z_1 = q_0 e^{i\vartheta_1}, \vartheta_1 \in (0, \frac{\pi}{2})$. Then, from (3.6), we have $\zeta_1 = q_0 e^{i\vartheta_1}, \zeta_2 = -q_0 e^{-i\vartheta_1}, \hat{\zeta}_1 = q_0 e^{-i\vartheta_1}, \hat{\zeta}_2 = -q_0 e^{i\vartheta_1}$. Let $q_- = q_0 e^{i\theta_-}, \theta_- \in \{0, \pi\}, b[\zeta_1] = b_1$, where b_1 is arbitrary parameter. From Proposition 2.5, we have $b[\zeta_2] = -\frac{1}{b_1^*}$. From Eq. (3.18), one has

$$\begin{aligned} s'_{22}(\zeta_1) &= \frac{\zeta_1 - \zeta_2}{(\zeta_1 - \hat{\zeta}_1)(\zeta_1 - \hat{\zeta}_2)} = \frac{\cos(\vartheta_1)}{2q_0 i e^{i\vartheta_1}\sin(\vartheta_1)}, \\ s'_{22}(\zeta_2) &= \frac{\zeta_2 - \zeta_1}{(\zeta_2 - \hat{\zeta}_1)(\zeta_2 - \hat{\zeta}_2)} = \frac{\cos(\vartheta_1)}{2q_0 i e^{-i\vartheta_1}\sin(\vartheta_1)}, \end{aligned} \tag{3.27}$$

then we have

$$\begin{aligned} A[\zeta_1] &= \frac{b[\zeta_1]}{s'_{22}(\zeta_1)} = \frac{2q_0 b_1 i e^{i\vartheta_1}\sin(\vartheta_1)}{\cos(\vartheta_1)}, \\ A[\zeta_2] &= \frac{b[\zeta_2]}{s'_{22}(\zeta_2)} = -\frac{2q_0 i e^{-i\vartheta_1}\sin(\vartheta_1)}{b_1^*\cos(\vartheta_1)}. \end{aligned} \tag{3.28}$$

Thus the one-simple pole solution of the nonlocal Hirota equation (2.3) is deduced as

$$q(x,t) = q_0 \frac{\Omega_1}{\Omega_2}, \tag{3.29}$$

$$\begin{aligned} \Omega_1 =& (2\sin(\vartheta_1) + ie^{i\vartheta_1})\cos(\vartheta_1)\Theta_1 - (2\sin(\vartheta_1) - ie^{-i\vartheta_1}) \\ & \times b_1 b_1^* \cos(\vartheta_1)\Theta_2 + b_1^*\cos(\vartheta_1)^2 e^{3i\theta_-} \\ & + 2ib_1\sin(\vartheta_1)\Theta_3(e^{-i\vartheta_1+i\theta_-} - e^{i\vartheta_1+i\theta_-}) \\ & + (3b_1\cos(\vartheta_1)^2 - 4b_1)\Theta_3 e^{i\theta_-}, \\ \Omega_2 =& i\cos(\vartheta_1)\Theta_1 e^{i\vartheta_1 - i\theta_-} + ib_1 b_1^*\cos(\vartheta_1)\Theta_2 e^{-i\vartheta_1 - i\theta_-} \\ & - \cos(\vartheta_1)^2 b_1\Theta_3 + b_1^*\cos(\vartheta_1)^2 e^{2i\theta_-}, \\ \Theta_1 =& e^{-4q_0\sin(\vartheta_1)(-\frac{1}{2}x - \beta q_0^2 t + i\delta q_0\cos(\vartheta_1)t - 2\beta q_0^2\cos(\vartheta_1)^2 t) - i\vartheta_1 + 2i\theta_-}, \\ \Theta_2 =& e^{4q_0\sin(\vartheta_1)(\frac{1}{2}x + \beta q_0^2 t + i\delta q_0\cos(\vartheta_1)t + 2\beta q_0^2\cos(\vartheta_1)^2 t) + i\vartheta_1 + 2i\theta_-}, \\ \Theta_3 =& e^{4q_0\sin(\vartheta_1)(x + 2\beta q_0^2 t + 4\beta q_0^2\cos(\vartheta_1)^2 t)}. \end{aligned} \tag{3.30}$$

In order to discuss the regularity of the above solution, we need to examine whether the denominator of Eq. (3.29) is zero under certain conditions. Without loss of generality, let $q_0 = 1, \theta_- = 0, b_1 = b_{11} + ib_{12}$, we have

$$\begin{aligned} |\Omega_2|^2 =& 2\cos(\vartheta_1)^2\Big(((-b_{11}^2 - b_{12}^2)\cos(8\sin(\vartheta_2)\delta\cos(\vartheta_1)t) \\ & + (b_{11}^2 - b_{12}^2)\cos(\vartheta_1)^2 - \frac{b_{11}^4}{2} - b_{11}^2 b_{12}^2 - \frac{b_{12}^4}{2} - \frac{1}{2})\Xi^2 \\ & + ((b_{12}(b_{11}^2 + b_{12}^2 + 1)\cos(4\sin(\vartheta_1)\delta\cos(\vartheta_1)t) \\ & + \sin(4\sin(\vartheta_1)\delta\cos(\vartheta_1)t)b_{11}(b_{11}^2 + b_{12}^2 - 1))\Xi \\ & + (b_{12}(b_{11}^2 + b_{12}^2 + 1)\cos(4\sin(\vartheta_1)\delta\cos(\vartheta_1)t) \\ & - \sin(4\sin(\vartheta_1)\delta\cos(\vartheta_1)t)b_{11}(b_{11}^2 + b_{12}^2 - 1))\Xi^3 \\ & - \frac{\cos(\vartheta_1)(b_{11}^2 + b_{12}^2)(A^4 + 1)}{2})\cos(\vartheta_1)\Big). \end{aligned} \tag{3.31}$$

where $\Xi = e^{4\sin(\vartheta_1)(\frac{1}{2}x + \beta t + 2\beta\cos(\vartheta_1)^2 t)}$. When $|\Omega_2|^2 = 0$, the solutions (3.29) have the singularity. For example, When $b_1 = 1$, Eq. (3.31) become

$$\begin{aligned} |\Omega_2|^2 =& \cos(\vartheta_1)^2\Big((-2\cos(\vartheta_1)^2 + 2\cos(8\sin(\vartheta_1)\delta\cos(\vartheta_1)t) + 2) \\ & \times e^{4\sin(\vartheta_1)(x + 2\beta t + 4\beta\cos(\vartheta_1)^2 t)} \\ & + \cos(\vartheta_1)^2(e^{8\sin(\vartheta_1)(x + 2\beta t + 4\beta\cos(\vartheta_1)^2 t)} + 1)\Big). \end{aligned} \tag{3.32}$$

When $-2\cos(\vartheta_1)^2 + 2\cos(8\sin(\vartheta_1)\delta\cos(\vartheta_1)t) + 2 \geq 0$, the soliton solution (3.29) can be regular, which means that the solution is nonsingular at the region of $\frac{1}{8\sin(\vartheta_1)\delta\cos(\vartheta_1)}(-\frac{\pi}{2} + 2n\pi) \leq t \leq \frac{1}{8\sin(\vartheta_1)\delta\cos(\vartheta_1)}(\frac{\pi}{2} + 2n\pi)$, and n is integer. Obviously, when $\delta \to 0, \vartheta_1 \to 0$ or $\frac{\pi}{2}$, the regular region will be whole plane.

Through choosing different parameters, the different dynamic behaviors are presented in Figs. 2–5. Of which, Fig. 2(a) (b) display a dark soliton, Fig. 2(c) describes the peak of wave along the line $t + 0.25x = 0$ which is the center trajectory. In Fig. 2(c), we find the crest is less than 1(the height of background wave) within a certain region, and beyond the region, the crest is greater than 1. As we can see from Fig. 3, as $|t|$ increases, the dark soliton turns into the anti-dark soliton, this fact can also be verified in Fig. 2(c). This phenomenon is quite interesting and original for the nonlocal Hirota equation (2.3). Fig. 4 shows a dark–anti-dark pair solution, and Fig. 5 exhibits a breather wave, which is singular at points $\{x = -\frac{\pi}{10} - \frac{n\pi}{5}, t = \frac{\pi}{4} + \frac{n\pi}{2}\}$, and n is integer. Meanwhile, comparing Fig. 2 and Fig. 4, we find that as the parameter b_1 increases, the dark soliton turns into the dark–anti-dark pair solution. On the other hand, from Figs. 2 and 5, we find that as parameter δ increases and parameter β decreases, the dark soliton changes into the breather wave.

Case 2: $N = 2$

Let $z_1 = q_0 e^{i\vartheta_1}, z_2 = q_0 e^{i\vartheta_2}, \vartheta_1, \vartheta_2 \in (0, \frac{\pi}{2})$. Let $q_- = q_0 e^{i\theta_-}, \theta_- \in \{0, \pi\}, b[\zeta_1] = b_1, b[\zeta_2] = b_2$, where b_1, b_2 are all arbitrary parameters. We obtain the two-simple pole solution, which displays the interaction of two dark–anti-dark pair solutions(see Fig. 6). As shown in Fig. 6, when $t = -5$ (before the interaction), the wave profile consists of two dark–anti-dark pair solutions, when $t = 0$ (they have the strong interaction), the wave profile creates two spikes. When $t = 5$ (after the interaction), the wave profile restores the original shape. Moreover, in

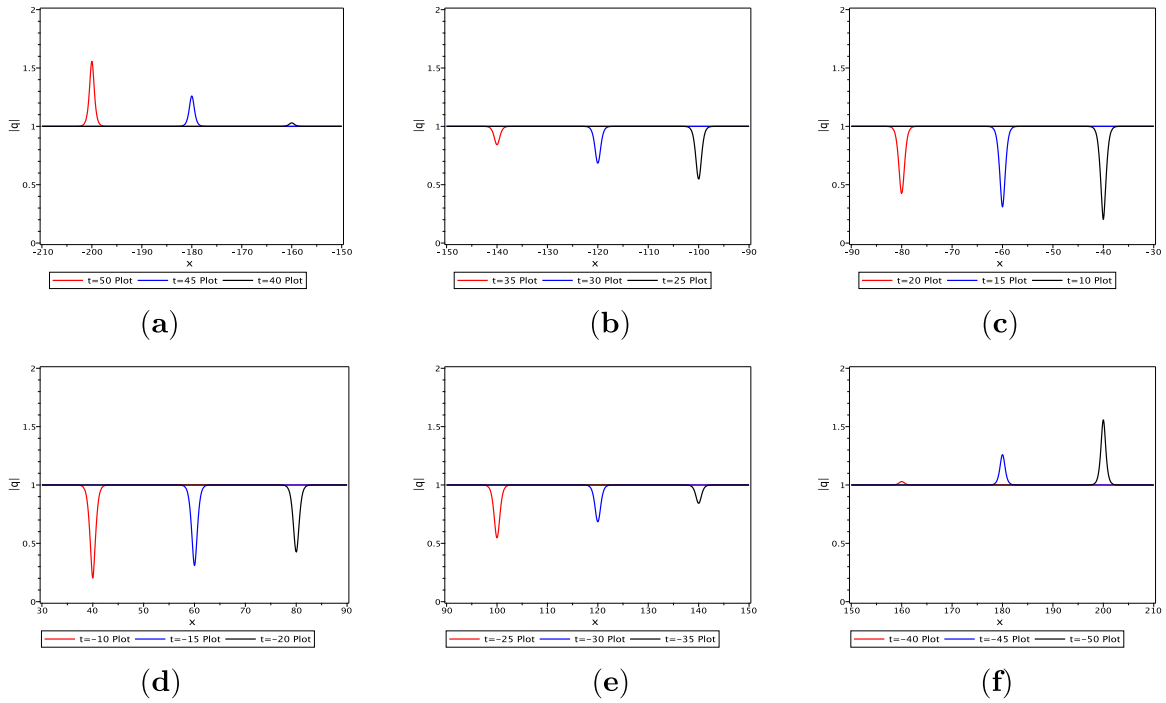

Fig. 3. The wave propagation of one-simple pole solution along the x-axis at different time. The parameters are $b_1 = 1, q_0 = 1, \vartheta_1 = \frac{\pi}{4}, \theta_- = 0, \delta = \frac{1}{100}, \beta = 1$.

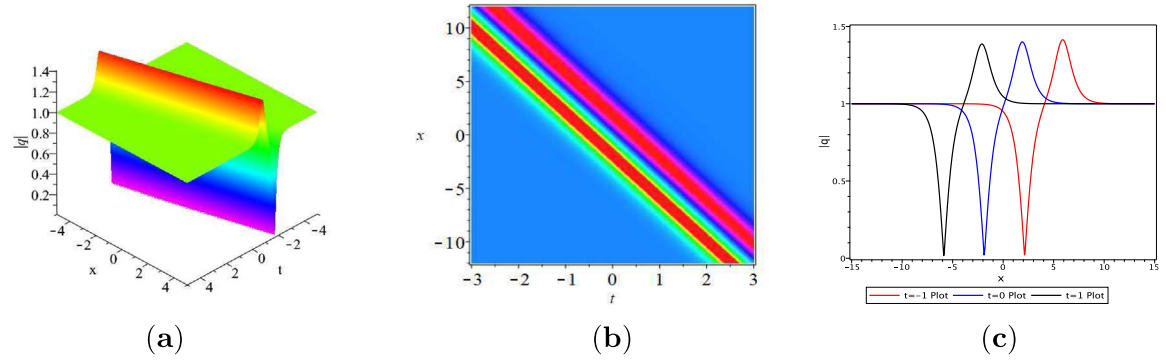

Fig. 4. One-simple pole solution for Eq. (2.3) with the parameters: $b_1 = 10, q_0 = 1, \vartheta_1 = \frac{\pi}{4}, \theta_- = 0, \delta = \frac{1}{100}, \beta = 1$. (**a**) Three dimensional plot; (**b**) The density plot; (**c**) The wave propagation along the x-axis at $t = -1$ (red), $t = 0$ (blue), $t = 1$ (black).

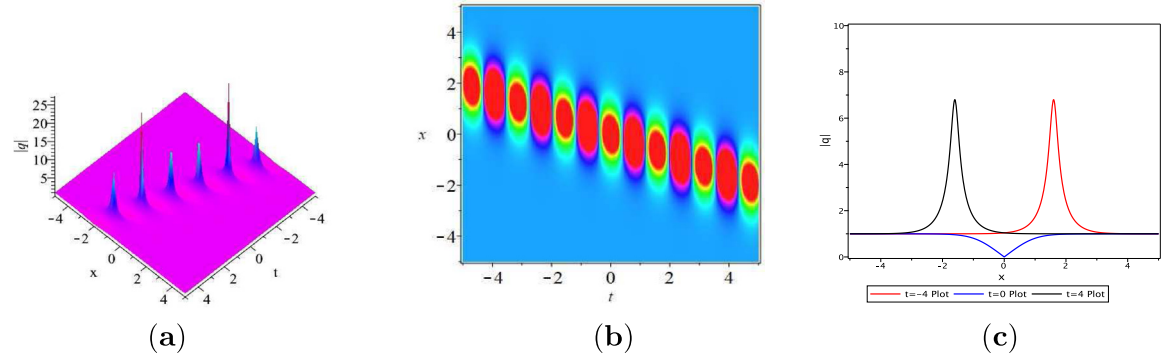

Fig. 5. One-simple pole solution for Eq. (2.3) with the parameters: $b_1 = 1, q_0 = 1, \vartheta_1 = \frac{\pi}{4}, \theta_- = 0, \delta = 1, \beta = \frac{1}{10}$. (**a**) Three dimensional plot; (**b**) The density plot; (**c**) The wave propagation along the x-axis at $t = -4$ (red), $t = 0$ (blue), $t = 4$ (black).

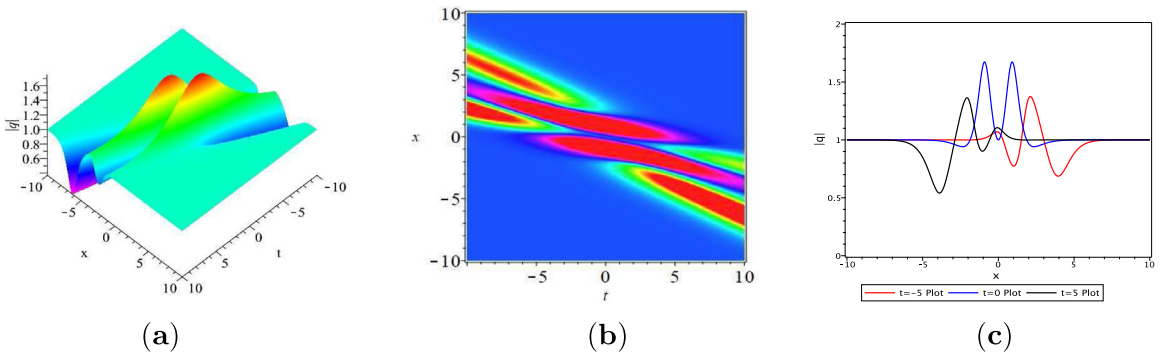

Fig. 6. The two-simple pole solution for Eq. (2.3) with the parameters: $b_1=-1, b_2=-1, q_0=1, \vartheta_1=\frac{\pi}{6}, \vartheta_2=\frac{\pi}{3}, \theta_-=0, \delta=\frac{1}{100}, \beta=\frac{1}{10}$. (**a**) Three dimensional plot; (**b**) The density plot; (**c**) The wave propagation along the x-axis at $t=-5$ (red), $t=0$ (blue), $t=5$ (black).

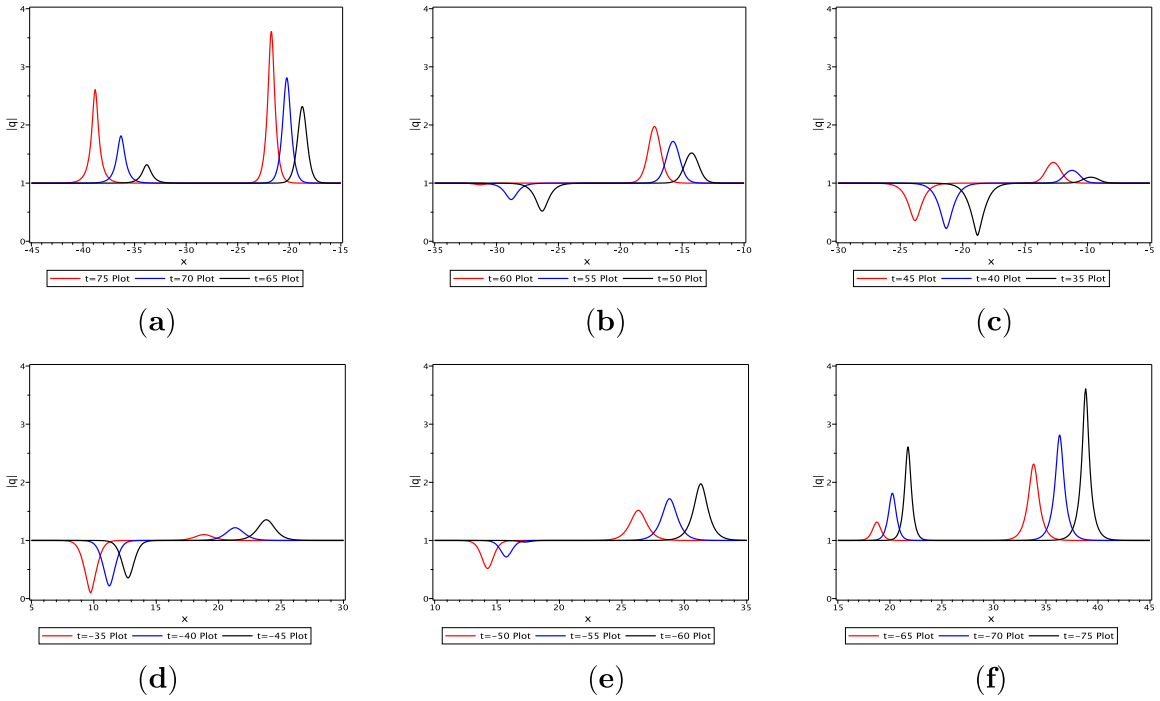

Fig. 7. The wave propagation of two-simple pole solution along the x-axis at different time. The parameters are $b_1=-1, b_2=-1, q_0=1, \vartheta_1=\frac{\pi}{6}, \vartheta_2=\frac{\pi}{3}, \theta_-=0, \delta=\frac{1}{100}, \beta=\frac{1}{10}$.

Fig. 7, when $|t|$ increases, the dark–anti-dark pair soliton degrades into the two anti-dark soliton.

4. The nonlocal hirota equation with NZBCs: double poles

4.1. Direct scattering problem

In this part, we suppose that the N discrete spectral points are double zeros of the scattering coefficients $s_{11}(z)$ and $s_{22}(z)$, that is, we have $s_{22}(z_0)=s'_{22}(z_0)=0$ and $s''_{22}(z_0)\neq 0$ for $z_0\in D_+\cap\{z\in\mathbb{C}:\mathrm{Re}z>0\}$.

Defining

$$b[z_0]=\frac{\Psi_{+2}(x,t,z_0)}{\Psi_{-1}(x,t,z_0)},$$
$$d[z_0]=\frac{\Psi'_{+2}(x,t;z_0)-b[z_0]\Psi'_{-1}(x,t;z_0)}{\Psi_{-1}(x,t;z_0)},\quad z_0\in\Upsilon\cap D_+,$$
$$b[z_0]=\frac{\Psi_{+1}(x,t,z_0)}{\Psi_{-2}(x,t,z_0)},$$
$$d[z_0]=\frac{\Psi'_{+1}(x,t;z_0)-b[z_0]\Psi'_{-2}(x,t;z_0)}{\Psi_{-2}(x,t;z_0)},\quad z_0\in\Upsilon\cap D_-,\tag{4.1}$$

we have

$$A[z_0]=\begin{cases}\frac{2b[z_0]}{s''_{22}(z_0)}, & z_0\in\Upsilon\cap D_+,\\ \frac{2b[z_0]}{s''_{11}(z_0)}, & z_0\in\Upsilon\cap D_-,\end{cases}$$
$$B[z_0]=\begin{cases}\frac{d[z_0]}{b[z_0]}-\frac{s'''_{22}(z_0)}{3s''_{22}(z_0)}, & z_0\in\Upsilon\cap D_+,\\ \frac{d[z_0]}{b[z_0]}-\frac{s'''_{11}(z_0)}{3s''_{11}(z_0)}, & z_0\in\Upsilon\cap D_-,\end{cases}\tag{4.2}$$

and

$$\underset{z=z_0}{L_{-2}}\left[\frac{\Psi_{+2}(x,t;z)}{s_{22}(z)}\right]=A[z_0]\Psi_{-1}(x,t;z_0),\quad z_0\in\Upsilon\cap D_+,$$
$$\underset{z=z_0}{L_{-2}}\left[\frac{\Psi_{+1}(x,t;z)}{s_{11}(z)}\right]=A[z_0]\Psi_{-2}(x,t;z_0),\quad z_0\in\Upsilon\cap D_-,$$
$$\underset{z=z_0}{\mathrm{Res}}\left[\frac{\Psi_{+2}(x,t;z)}{s_{22}(z)}\right]=A[z_0]\left[\Psi'_{-1}(x,t;z_0)+B[z_0]\Psi_{-1}(x,t;z_0)\right],$$

$$z_0 \in \Upsilon \cap D_+,$$
$$\operatorname*{Res}_{z=z_0}\left[\frac{\Psi_{+1}(x,t;z)}{s_{11}(z)}\right] = A[z_0]\left[\Psi'_{-2}(x,t;z_0) + B[z_0]\Psi_{-2}(x,t;z_0)\right],$$
$$z_0 \in \Upsilon \cap D_-. \tag{4.3}$$

Proposition 4.1. *Two relations for $b[z_0]$, $d[z_0]$, $s_{22}^{(m)}(z_0)$ and $s_{11}^{(m)}(z_0)$ are derived below:*

- *The first relation*

$$b[z_0] = -\frac{1}{b[-z_0^*]^*}, \quad d[z_0] = -\frac{d[-z_0^*]^*}{b^2[-z_0^*]^*},$$
$$s_{11}^{(m)}(z_0) = (-1)^m s_{11}^{(m)}(-z_0^*)^*, \quad s_{22}^{(m)}(z_0) = (-1)^m s_{22}^{(m)}(-z_0^*)^*, \ m \in \mathbb{N}. \tag{4.4}$$

- *The second relation*

$$b[z_0] = -\frac{q_+}{q_-^*} b[\frac{q_0^2}{z_0}], \quad d[z_0] = \frac{q_+ q_-}{z_0^2} d[\frac{q_0^2}{z_0}],$$
$$s_{22}^{(m)}(z_0) = (-\frac{q_0^2}{z_0^2})^m s_{11}^{(m)}(\frac{q_0^2}{z_0}), \quad z_0 \in D_+,$$
$$b[z_0] = -\frac{q_+^*}{q_-} b[\frac{q_0^2}{z_0}], \quad d[z_0] = \frac{q_+^* q_-^*}{z_0^2} d[\frac{q_0^2}{z_0}],$$
$$s_{11}^{(m)}(z_0) = (-\frac{q_0^2}{z_0^2})^m s_{22}^{(m)}(\frac{q_0^2}{z_0}), \quad z_0 \in D_-. \tag{4.5}$$

4.2. Inverse problem with NZBCs and double poles

By subtracting out the asymptotic values as $z \to \infty, z \to 0$, the residue, and the coefficient L_{-2} from the original non-regular RHP, one can obtain the following regular RHP

$$M_- + \frac{i}{z}\sigma_3 Q_- - I -$$
$$\sum_{n=1}^{2N}\left[\frac{L_{-2}M_+}{(z-\zeta_n)^2} + \frac{\operatorname{Res}M_+}{z-\zeta_n} + \frac{L_{-2}M_-}{(z-\hat{\zeta}_n)^2} + \frac{\operatorname{Res}M_-}{z-\hat{\zeta}_n}\right] =$$
$$M_+ + \frac{i}{z}\sigma_3 Q_- - I -$$
$$\sum_{n=1}^{2N}\left[\frac{L_{-2}M_+}{(z-\zeta_n)^2} + \frac{\operatorname{Res}M_+}{z-\zeta_n} + \frac{L_{-2}M_-}{(z-\hat{\zeta}_n)^2} + \frac{\operatorname{Res}M_-}{z-\hat{\zeta}_n}\right] - M_+ G. \tag{4.6}$$

Via the Plemelj's formulae, the above RHP can be solved as

$$M(x,t;z) = I - \frac{i}{z}\sigma_3 Q_- + \frac{1}{2\pi i}\int_\Sigma \frac{M_+(x,t;\zeta)G(x,t;\zeta)}{\zeta - z}d\zeta$$
$$+\sum_{n=1}^{2N}\left[\frac{L_{-2}M_+}{(z-\zeta_n)^2} + \frac{\operatorname{Res}M_+}{z-\zeta_n} + \frac{L_{-2}M_-}{(z-\hat{\zeta}_n)^2} + \frac{\operatorname{Res}M_-}{z-\hat{\zeta}_n}\right]. \tag{4.7}$$

The residue and the coefficient L_{-2} of $M(x,t;z)$ in Eq. (4.7) can be written as

$$\underset{z=\zeta_n}{L_{-2}M_+} = \left(0, A[\zeta_n]e^{-2i\theta(x,t;\zeta_n)}\mu_{-1}(x,t;\zeta_n)\right),$$
$$\underset{z=\hat{\zeta}_n}{L_{-2}M_-} = \left(A[\hat{\zeta}_n]e^{2i\theta(x,t;\hat{\zeta}_n)}\mu_{-2}(x,t;\hat{\zeta}_n), 0\right),$$
$$\underset{z=\zeta_n}{\operatorname{Res}M_+} = \Big(0, A[\zeta_n]e^{-2i\theta(x,t;\zeta_n)}\left[\mu'_{-1}(x,t;\zeta_n)\right.$$
$$\left.+\left[B[\zeta_n] - 2i\theta'(x,t;\zeta_n)\right]\mu_{-1}(x,t;\zeta_n)\right]\Big),$$
$$\underset{z=\hat{\zeta}_n}{\operatorname{Res}M_-} = \Big(A[\hat{\zeta}_n]e^{2i\theta(x,t;\hat{\zeta}_n)}\Big[\mu'_{-2}(x,t;\hat{\zeta}_n)$$
$$+\left[B[\hat{\zeta}_n] + 2i\theta'(x,t;\hat{\zeta}_n)\right]\mu_{-2}(x,t;\hat{\zeta}_n)\Big], 0\Big). \tag{4.8}$$

Then, one has

$$\frac{\underset{z=\zeta_n}{L_{-2}M_+}}{(z-\zeta_n)^2} + \frac{\underset{z=\zeta_n}{\operatorname{Res}M_+}}{z-\zeta_n} + \frac{\underset{z=\hat{\zeta}_n}{L_{-2}M_-}}{(z-\hat{\zeta}_n)^2} + \frac{\underset{z=\hat{\zeta}_n}{\operatorname{Res}M_-}}{z-\hat{\zeta}_n} =$$
$$\left(\hat{C}_n(z)\left[\mu'_{-2}(\hat{\zeta}_n) + \left(\hat{D}_n + \frac{1}{z-\hat{\zeta}_n}\right)\mu_{-2}(\hat{\zeta}_n)\right],\right.$$
$$\left.C_n(z)\left[\mu'_{-1}(\zeta_n) + \left(D_n + \frac{1}{z-\zeta_n}\right)\mu_{-1}(\zeta_n)\right]\right), \tag{4.9}$$

and

$$C_n(z) = \frac{A[\zeta_n]e^{-2i\theta(\zeta_n)}}{z-\zeta_n}, \quad D_n = B[\zeta_n] - 2i\theta'(\zeta_n),$$
$$\hat{C}_n(z) = \frac{A[\hat{\zeta}_n]e^{2i\theta(\hat{\zeta}_n)}}{z-\hat{\zeta}_n}, \quad \hat{D}_n = B[\hat{\zeta}_n] + 2i\theta'(\hat{\zeta}_n). \tag{4.10}$$

Moreover, according to (3.4), we obtain

$$M^{(1)}(x,t;z) = -\frac{1}{2\pi i}\int_\Sigma M_+(x,t;\zeta)G(x,t;\zeta)d\zeta - i\sigma_3 Q_-$$
$$+\sum_{n=1}^{2N}\left(A[\hat{\zeta}_n]e^{2i\theta(\hat{\zeta}_n)}\left(\mu'_{-2}(\hat{\zeta}_n) + \hat{D}_n\mu_{-2}(\hat{\zeta}_n)\right),\right.$$
$$\left.A[\zeta_n]e^{-2i\theta(\zeta_n)}\left(\mu'_{-1}(\zeta_n) + D_n\mu_{-1}(\zeta_n)\right)\right). \tag{4.11}$$

The potential $q(x,t)$ with double poles for the nonlocal Hirota equation with NZBCs is given by

$$q(x,t) = iM_{12}^{(1)} = q_- - \frac{1}{2\pi}\int_\Sigma (M_+(x,t;\zeta)G(x,t;\zeta))_{12}d\zeta$$
$$+i\sum_{n=1}^{2N}A[\zeta_n]e^{-2i\theta(\zeta_n)}\left(\mu'_{-11}(\zeta_n) + D_n\mu_{-11}(\zeta_n)\right). \tag{4.12}$$

4.3. Trace formula and theta condition

The scattering coefficients $s_{22}(z)$ and $s_{11}(z)$ respectively have simple zeros ζ_n and $\hat{\zeta}_n$, thus we can take

$$\beta^+(z) = s_{22}(z)\prod_{n=1}^{2N}(\frac{z-\hat{\zeta}_n}{z-\zeta_n})^2, \ \beta^-(z) = s_{11}(z)\prod_{n=1}^{2N}(\frac{z-\zeta_n}{z-\hat{\zeta}_n})^2, \tag{4.13}$$

that means $\beta^+(z)$ is analytic and has no zeros in D_+, and $\beta^-(z)$ is analytic and has no zeros in D_-. Also, $\beta^\pm(z) \to o(1)$ as $z \to \infty$. According to the Plemelj's formulae, $\beta^\pm(z)$ can be written as

$$\log\beta^\pm(z) = \mp\frac{1}{2\pi i}\int_\Sigma \frac{\log(1-\rho\tilde{\rho})}{s-z}ds, \quad z \in D^\pm. \tag{4.14}$$

Using Eq. (4.13), we derive the following trace formulae

$$s_{22}(z) = \exp\left[-\frac{1}{2\pi i}\int_\Sigma \frac{\log(1-\rho\tilde{\rho})}{s-z}ds\right]\prod_{n=1}^{2N}(\frac{z-\zeta_n}{z-\hat{\zeta}_n})^2,$$
$$s_{11}(z) = \exp\left[\frac{1}{2\pi i}\int_\Sigma \frac{\log(1-\rho\tilde{\rho})}{s-z}ds\right]\prod_{n=1}^{2N}(\frac{z-\hat{\zeta}_n}{z-\zeta_n})^2. \tag{4.15}$$

Let $z \to 0$ in the first formula of Eq. (4.15), one has

$$\exp\left[\frac{i}{2\pi}\int_\Sigma \frac{\log(1-\rho\tilde{\rho})}{s}ds\right]\prod_{n=1}^{N}\frac{|z_n|^8}{q_0^8} = 1. \tag{4.16}$$

In addition, taking the derivative of Eq. (4.15) twice with respect to z, we obtain $s'_{22}(\zeta_j)$ and $s'_{11}(\hat{\zeta}_j)$, given by

$$s''_{22}(\zeta_j) = \exp\left[-\frac{1}{2\pi i}\int_\Sigma \frac{\log(1-\rho\tilde{\rho})}{s-\zeta_j}ds\right]\frac{\prod_{m\neq j}2(\zeta_j-\zeta_m)^2}{\prod_{m=1}^{2N}(\zeta_j-\hat{\zeta}_m)^2},$$

$$s_{11}''(\hat{\zeta}_j)=\exp\left[\frac{1}{2\pi i}\int_{\Sigma}\frac{\log(1-\rho\tilde{\rho})}{s-\hat{\zeta}_j}ds\right]\frac{\prod_{m\neq j}2(\hat{\zeta}_j-\hat{\zeta}_m)^2}{\prod_{m=1}^{2N}(\hat{\zeta}_j-\zeta_m)^2}. \quad (4.17)$$

Notice that the general expressions of the $s_{22}'''(\zeta_j)$, $s_{11}'''(\hat{\zeta}_j)$ are very complicated, and we omit them here. However, with the aid of computer softwares such as Maple and Matlab, one can easily get the corresponding exact expressions by taking the third derivative of the Eq. (4.15) with respect to z.

4.4. Double poles soliton solutions of nonlocal hirota equation under NZBCs

In this subsection, for the case of double poles with reflectionless potential, we first need to evaluate $\mu_{-1}'(\zeta_n)$, $\mu_{-1}(\zeta_n)$, $\mu_{-2}'(\zeta_n)$, $\mu_{-2}(\zeta_n)$. When $\rho(z)=\tilde{\rho}(z)=0$, the second column of Eq. (4.7) meets

$$\mu_{-2}(z)=\begin{pmatrix}-\frac{i}{z}q_-\\1\end{pmatrix}+\sum_{n=1}^{2N}C_n(z)\left[\mu_{-1}'(\zeta_n)+\left(D_n+\frac{1}{z-\zeta_n}\right)\mu_{-1}(\zeta_n)\right], \quad (4.18)$$

$$\mu_{-2}'(z)=\begin{pmatrix}\frac{i}{z^2}q_-\\0\end{pmatrix}-\sum_{n=1}^{2N}\frac{C_n(z)}{z-\zeta_n}\left[\mu_{-1}'(\zeta_n)+\left(D_n+\frac{2}{z-\zeta_n}\right)\mu_{-1}(\zeta_n)\right]. \quad (4.19)$$

We take the first-order derivative about z in formula (3.20), given by

$$\mu_{-2}'(z)=\frac{iq_-}{z^2}\mu_{-1}(\frac{q_0^2}{z})+\frac{iq_0^2q_-}{z^3}\mu_{-1}'(\frac{q_0^2}{z}). \quad (4.20)$$

Substituting Eqs. (3.20) and (4.20) into Eqs. (4.18) and (4.19), and letting $z=\hat{\zeta}_j, j=1,2,\ldots,2N$, we obtain the following $4N$ linear system

$$\sum_{n=1}^{2N}\left\{C_n(\hat{\zeta}_j)\mu_{-1}'(\zeta_n)+\left[C_n(\hat{\zeta}_j)\left(D_n+\frac{1}{\hat{\zeta}_j-\zeta_n}\right)+\frac{iq_-}{\hat{\zeta}_j}\delta_{j,n}\right]\mu_{-1}(\zeta_n)\right\}=\begin{pmatrix}\frac{i}{\hat{\zeta}_j}q_-\\-1\end{pmatrix}, \quad (4.21)$$

$$\sum_{n=1}^{2N}\left\{\left(\frac{C_n(\hat{\zeta}_j)}{\hat{\zeta}_j-\zeta_n}+\frac{iq_0^2q_-}{\hat{\zeta}_j^3}\delta_{j,n}\right)\mu_{-1}'(\zeta_n)+\left[\frac{C_n(\hat{\zeta}_j)}{\hat{\zeta}_j-\zeta_n}\left(D_n+\frac{2}{\hat{\zeta}_j-\zeta_n}\right)+\frac{iq_-}{\hat{\zeta}_j^2}\delta_{j,n}\right]\mu_{-1}(\zeta_n)\right\}=\begin{pmatrix}\frac{i}{\hat{\zeta}_j^2}q_-\\0\end{pmatrix}. \quad (4.22)$$

Theorem 4.1. *The general formula of the double poles solution for the nonlocal Hirota (2.3) with NZBCs (2.4) is expressed as*

$$q(x,t)=q_--i\frac{\det\begin{pmatrix}\mathcal{G}&\psi\\\omega^T&0\end{pmatrix}}{\det(\mathcal{G})}. \quad (4.23)$$

Proof. According to Eqs. (4.21) and (4.22), we easily obtain a $4N$ linear system with respect to $\mu_{-11}(\zeta_n)$, $\mu_{-11}'(\zeta_n)$

$$\sum_{n=1}^{2N}\left\{C_n(\hat{\zeta}_j)\mu_{-11}'(\zeta_n)+\left[C_n(\hat{\zeta}_j)\left(D_n+\frac{1}{\hat{\zeta}_j-\zeta_n}\right)+\frac{iq_-}{\hat{\zeta}_j}\delta_{j,n}\right]\mu_{-11}(\zeta_n)\right\}=\frac{iq_-}{\hat{\zeta}_j}, \quad (4.24)$$

$$\sum_{n=1}^{2N}\left\{\left(\frac{C_n(\hat{\zeta}_j)}{\hat{\zeta}_j-\zeta_n}+\frac{iq_0^2q_-}{\hat{\zeta}_j^3}\delta_{j,n}\right)\mu_{-11}'(\zeta_n)+\left[\frac{C_n(\hat{\zeta}_j)}{\hat{\zeta}_j-\zeta_n}\left(D_n+\frac{2}{\hat{\zeta}_j-\zeta_n}\right)+\frac{iq_-}{\hat{\zeta}_j^2}\delta_{j,n}\right]\mu_{-11}(\zeta_n)\right\}=\frac{iq_-}{\hat{\zeta}_j^2}, \quad (4.25)$$

the above linear system can be denoted in the matrix form:

$$\mathcal{G}\eta=\psi, \quad (4.26)$$

where

$$\psi=\begin{pmatrix}\psi^{(1)}\\\psi^{(2)}\end{pmatrix},\ \psi^{(1)}=(\frac{iq_-}{\hat{\zeta}_1},\frac{iq_-}{\hat{\zeta}_2},\ldots,\frac{iq_-}{\hat{\zeta}_{2N}})^T,$$
$$\psi^{(2)}=(\frac{iq_-}{\hat{\zeta}_1^2},\frac{iq_-}{\hat{\zeta}_2^2},\ldots,\frac{iq_-}{\hat{\zeta}_{2N}^2})^T,$$
$$\eta=\begin{pmatrix}\eta^{(1)}\\\eta^{(2)}\end{pmatrix},\ \eta^{(1)}=(\mu_{-11}(\zeta_1),\mu_{-11}(\zeta_2),\ldots,\mu_{-11}(\zeta_{2N}))^T,$$
$$\eta^{(2)}=(\mu_{-11}'(\zeta_1),\mu_{-11}'(\zeta_2),\ldots,\mu_{-11}'(\zeta_{2N}))^T,$$
$$\mathcal{G}=\begin{pmatrix}\mathcal{G}^{(11)}&\mathcal{G}^{(12)}\\\mathcal{G}^{(21)}&\mathcal{G}^{(22)}\end{pmatrix}, \quad (4.27)$$

with $\mathcal{G}^{(im)}=\left(\mathcal{G}_{jn}^{(im)}\right)_{2N\times 2N}(i,m=1,2)$ given by

$$\mathcal{G}_{jn}^{(11)}=C_n(\hat{\zeta}_j)\left(D_n+\frac{1}{\hat{\zeta}_j-\zeta_n}\right)+\frac{iq_-}{\hat{\zeta}_j}\delta_{j,n},\quad \mathcal{G}_{jn}^{(12)}=C_n(\hat{\zeta}_j),$$
$$\mathcal{G}_{jn}^{(21)}=\frac{C_n(\hat{\zeta}_j)}{\hat{\zeta}_j-\zeta_n}\left(D_n+\frac{2}{\hat{\zeta}_j-\zeta_n}\right)+\frac{iq_-}{\hat{\zeta}_j^2}\delta_{j,n},$$
$$\mathcal{G}_{jn}^{(22)}=\frac{C_n(\hat{\zeta}_j)}{\hat{\zeta}_j-\zeta_n}+\frac{iq_0^2q_-}{\hat{\zeta}_j^3}\delta_{j,n}. \quad (4.28)$$

At the case of reflectionless potential, Eq. (4.12) can be defined as

$$q=q_-+i\omega^T\eta, \quad (4.29)$$

where

$$\omega=\begin{pmatrix}\omega^{(1)}\\\omega^{(2)}\end{pmatrix},\ \omega^{(2)}=(A[\zeta_1]e^{-2i\theta(\zeta_1)},A[\zeta_2]e^{-2i\theta(\zeta_2)},$$
$$\ldots,A[\zeta_{2N}]e^{-2i\theta(\zeta_{2N})})^T,$$
$$\omega^{(1)}=(A[\zeta_1]e^{-2i\theta(\zeta_1)}D_1,A[\zeta_2]e^{-2i\theta(\zeta_2)}D_2,\ldots,A[\zeta_{2N}]e^{-2i\theta(\zeta_{2N})}D_{2N})^T. \quad (4.30)$$

From Eqs. (4.26), we get the expression of the double poles soliton solution. □

For example, we have the one-double poles soliton solution of the nonlocal Hirota equation with NZBCs when $N=1$. Let $z_1=q_0e^{i\vartheta_1}$, $\vartheta_1\in(0,\frac{\pi}{2})$. Then, from (3.6), we have $\zeta_1=q_0e^{i\vartheta_1}$, $\zeta_2=-q_0e^{-i\vartheta_1}$, $\hat{\zeta}_1=q_0e^{-i\vartheta_1}$, $\hat{\zeta}_2=-q_0e^{i\vartheta_1}$. Let $q_-=q_0e^{i\theta_-}$, $\theta_-\in\{0,\pi\}$, $b[\zeta_1]=b_1, d[\zeta_1]=d_1$, where b_1,d_1 are all arbitrary parameters. From Proposition 4.1, we have $b[\zeta_2]=-\frac{1}{b_1^*}$, $d[\zeta_2]=-(\frac{d_1}{b_1^2})^*$. From Eq. (4.17), one has

$$s_{22}''(\zeta_1)=\frac{2(\zeta_1-\zeta_2)^2}{(\zeta_1-\hat{\zeta}_1)^2(\zeta_1-\hat{\zeta}_2)^2}=\frac{(\cos(\vartheta_1))^2}{2(q_0ie^{i\vartheta_1}\sin(\vartheta_1))^2},$$
$$s_{22}''(\zeta_2)=\frac{2(\zeta_2-\zeta_1)^2}{(\zeta_2-\hat{\zeta}_1)^2(\zeta_2-\hat{\zeta}_2)^2}=\frac{(\cos(\vartheta_1))^2}{2(q_0ie^{-i\vartheta_1}\sin(\vartheta_1))^2}, \quad (4.31)$$

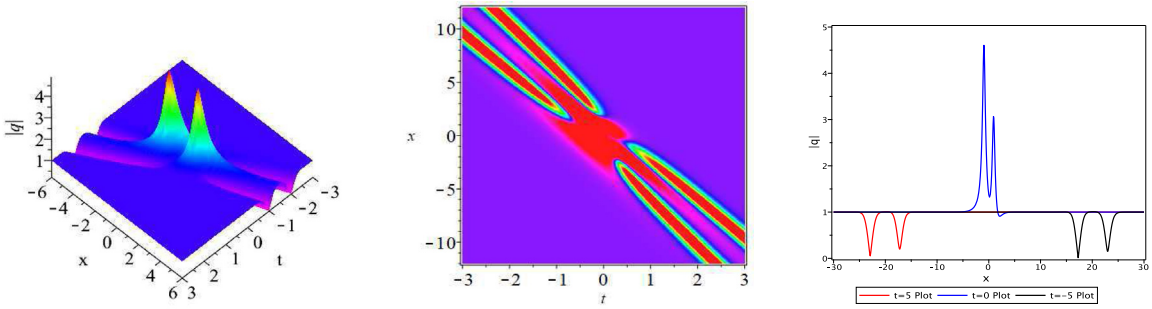

Fig. 8. The one-double poles solution for Eq. (2.3) with the parameters: $b_1 = 1, d_1 = 1, q_0 = 1, \vartheta_1 = \frac{\pi}{4}, \theta_- = 0, \delta = \frac{1}{100}, \beta = 1$. (**a**) Three dimensional plot; (**b**) The density plot; (**c**) The wave propagation along the x-axis at $t = -5$ (black), $t = 0$ (blue), $t = 5$ (red).

and through Maple computation, we get

$$s'''_{22}(\zeta_1) = \frac{12(\zeta_1-\zeta_2)(2\zeta_1\zeta_2-\zeta_1^2-(\hat{\zeta}_1+\hat{\zeta}_2)\zeta_2+\hat{\zeta}_1\hat{\zeta}_2)}{(\zeta_1-\hat{\zeta}_1)^3(\zeta_1-\hat{\zeta}_2)^3},$$
$$s'''_{22}(\zeta_2) = \frac{12(\zeta_2-\zeta_1)(2\zeta_1\zeta_2-\zeta_2^2-(\hat{\zeta}_1+\hat{\zeta}_2)\zeta_1+\hat{\zeta}_1\hat{\zeta}_2)}{(\zeta_2-\hat{\zeta}_1)^3(\zeta_2-\hat{\zeta}_2)^3}, \quad (4.32)$$

then using Eq. (4.2), we can derive the $A[\zeta_1], A[\zeta_2], B[\zeta_1], B[\zeta_2]$. Thus the one-double poles solution of the nonlocal Hirota equation (2.3) is deduced as

$$q(x,t) = q_- - i\frac{\det\begin{pmatrix} \mathcal{G}_{11}^{(11)} & \mathcal{G}_{12}^{(11)} & \mathcal{G}_{11}^{(12)} & \mathcal{G}_{12}^{(12)} & \psi_1^{(1)} \\ \mathcal{G}_{21}^{(11)} & \mathcal{G}_{22}^{(11)} & \mathcal{G}_{21}^{(12)} & \mathcal{G}_{22}^{(12)} & \psi_2^{(1)} \\ \mathcal{G}_{11}^{(21)} & \mathcal{G}_{12}^{(21)} & \mathcal{G}_{11}^{(22)} & \mathcal{G}_{12}^{(22)} & \psi_1^{(2)} \\ \mathcal{G}_{21}^{(21)} & \mathcal{G}_{22}^{(21)} & \mathcal{G}_{21}^{(22)} & \mathcal{G}_{22}^{(22)} & \psi_2^{(2)} \\ \omega_1^{(1)} & \omega_2^{(1)} & \omega_1^{(2)} & \omega_2^{(2)} & 0 \end{pmatrix}}{\det\begin{pmatrix} \mathcal{G}_{11}^{(11)} & \mathcal{G}_{12}^{(11)} & \mathcal{G}_{11}^{(12)} & \mathcal{G}_{12}^{(12)} \\ \mathcal{G}_{21}^{(11)} & \mathcal{G}_{22}^{(11)} & \mathcal{G}_{21}^{(12)} & \mathcal{G}_{22}^{(12)} \\ \mathcal{G}_{11}^{(21)} & \mathcal{G}_{12}^{(21)} & \mathcal{G}_{11}^{(22)} & \mathcal{G}_{12}^{(22)} \\ \mathcal{G}_{21}^{(21)} & \mathcal{G}_{22}^{(21)} & \mathcal{G}_{21}^{(22)} & \mathcal{G}_{22}^{(22)} \end{pmatrix}}, \quad (4.33)$$

where

$$\mathcal{G}_{jn}^{(11)} = C_n(\hat{\zeta}_j)\left(D_n + \frac{1}{\hat{\zeta}_j-\zeta_n}\right) + \frac{iq_-}{\hat{\zeta}_j}\delta_{j,n}, \quad \mathcal{G}_{jn}^{(12)} = C_n(\hat{\zeta}_j),$$
$$\mathcal{G}_{jn}^{(21)} = \frac{C_n(\hat{\zeta}_j)}{\hat{\zeta}_j-\zeta_n}\left(D_n + \frac{2}{\hat{\zeta}_j-\zeta_n}\right) + \frac{iq_-}{\hat{\zeta}_j^2}\delta_{j,n},$$
$$\mathcal{G}_{jn}^{(22)} = \frac{C_n(\hat{\zeta}_j)}{\hat{\zeta}_j-\zeta_n} + \frac{iq_0^2q_-}{\hat{\zeta}_j^3}\delta_{j,n},$$
$$C_n(\hat{\zeta}_j) = \frac{A[\zeta_n]e^{-2i\theta(\zeta_n)}}{\hat{\zeta}_j-\zeta_n}, \quad D_n = B[\zeta_n] - 2i\theta'(\zeta_n),$$
$$\omega_j^{(1)} = A[\zeta_j]e^{-2i\theta(\zeta_j)}D_j, \ \omega_j^{(2)} = A[\zeta_j]e^{-2i\theta(\zeta_j)},$$
$$\psi_j^{(1)} = \frac{iq_-}{\hat{\zeta}_j}, \ \psi_j^{(2)} = \frac{iq_-}{\hat{\zeta}_j^2},$$
$$\theta(\zeta_j) = \frac{(\zeta_j^2-q_0^2)\left[\beta t(q_0^4+4q_0^2\zeta_j^2+\zeta_j^4)+i\delta\zeta_j t(q_0^2+\zeta_j^2)+x\zeta_j^2\right]}{2\zeta_j^3},$$
$$j,n = 1,2,$$
$$\theta'(\zeta_j) = \frac{3\beta t(q_0^6+q_0^4\zeta_j^2+q_0^2\zeta_j^4+\zeta_j^6)+2i\delta\zeta_j t(q_0^4+\zeta_j^4)+\zeta_j^2x(q_0^2+\zeta_j^2)}{2\zeta_j^4}. \quad (4.34)$$

As a matter of convenience, we take $b_1 = 1, d_1 = 1, q_0 = 1, \vartheta_1 = \frac{\pi}{4}, \theta_- = 0, \delta = \frac{1}{100}, \beta = 1$ as an example to illustrate the correlative dynamic behavior for the one-double poles solution for nonlocal Hirota equation with NZBCs via image simulation. As displayed in Fig. 8, before the interaction $t = -5$, the wave profile contains two dark solitons, then they happen the strong collision at $t = 0$. After that, the wave profile becomes a two dark soliton again. Moreover, in Fig. 9, when $|t|$ increases, the two dark soliton degrades into the two anti-dark soliton.

Furthermore, we analyze the asymptotic states of the one-double poles solution as $t \to \pm\infty$ under $b_1 = 1, d_1 = 1, q_0 = 1, \vartheta_1 = \frac{\pi}{4}, \theta_- = 0, \delta = 0, \beta = 1$. Through analyzing the expression of the solution, we know the two characteristic curves are $x = -4t + \frac{\sqrt{2}}{2}\log(t)$ and $x = -4t - \frac{\sqrt{2}}{2}\log(t)$, respectively. Using maple symbol calculations, we can derive the long-time asymptotic state of the one-double poles solution as moving along these two characteristic curves, given by

$$|q(x,t)|^2 \to \frac{(128-e^{2\sqrt{2}(x+4t-\frac{\sqrt{2}}{2}\log(t))})^2}{(128+e^{2\sqrt{2}(x+4t-\frac{\sqrt{2}}{2}\log(t))})^2+512e^{2\sqrt{2}(x+4t-\frac{\sqrt{2}}{2}\log(t))}} + \frac{(128-e^{-2\sqrt{2}(x+4t+\frac{\sqrt{2}}{2}\log(t))})^2}{(128+e^{-2\sqrt{2}(x+4t+\frac{\sqrt{2}}{2}\log(t))})^2+512e^{-2\sqrt{2}(x+4t+\frac{\sqrt{2}}{2}\log(t))}}, \text{ as } t \to \infty. \quad (4.35)$$

From the above expression, it is not hard to see that the one-double poles solution reduces into the two dark one-soliton solution as $t \to \infty$, and when $t \to \infty$, the position shift of two dark one-soliton solution is $\sqrt{2}\log(t)$, which depends on t. We also select three different time $t = 20, t = 40, t = 60$ to verify the above asymptotic expressions by numerical plotting in Fig. 10. Numerical results show that the exact solution and the asymptotic solution are almost identical.

5. The data-driven soliton solutions for the nonlocal hirota equation via PINN algorithm

In this section, the PINN algorithm is used to learn the soliton solutions for the nonlocal Hirota equation (2.3) with Dirichlet boundary conditions, given by

$$\begin{cases} q_t + \delta\left[q_{xx} - 2q^2q^*(-x,-t) + 2q_0^2q\right] \\ +\beta\left[q_{xxx} - 6qq^*(-x,-t)q_x\right] = 0, \\ x \in [x_0, x_1], \quad t \in [t_0, t_1], \quad q(x,t_0) = q_0(x), \\ q(x_0,t) = q_{lb}(t), \ q(x_1,t) = q_{ub}(t), \end{cases} \quad (5.1)$$

where x_0, x_1 denote the corresponding boundaries of x, t_0, t_1 are initial and final times of t. The $q_0(x)$ defines the initial condition.

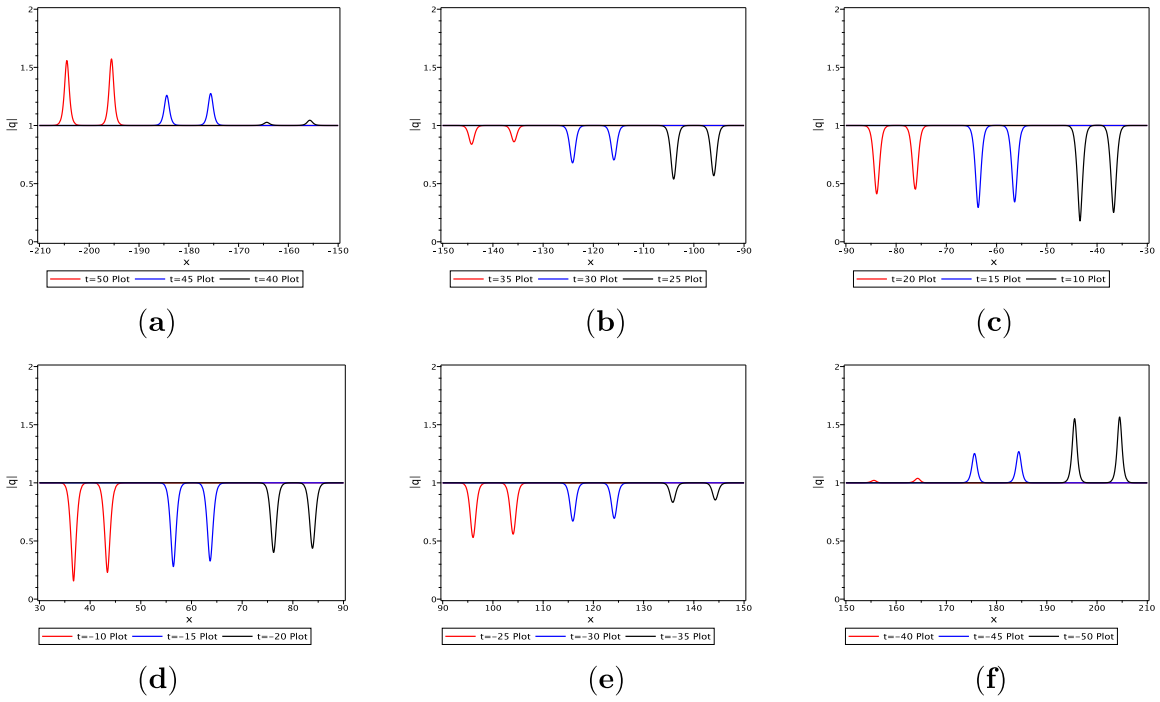

Fig. 9. The wave propagation of one-double poles solution along the x-axis at different time. The parameters are $b_1 = 1, d_1 = 1, q_0 = 1, \vartheta_1 = \frac{\pi}{4}, \theta_- = 0, \delta = \frac{1}{100}, \beta = 1$.

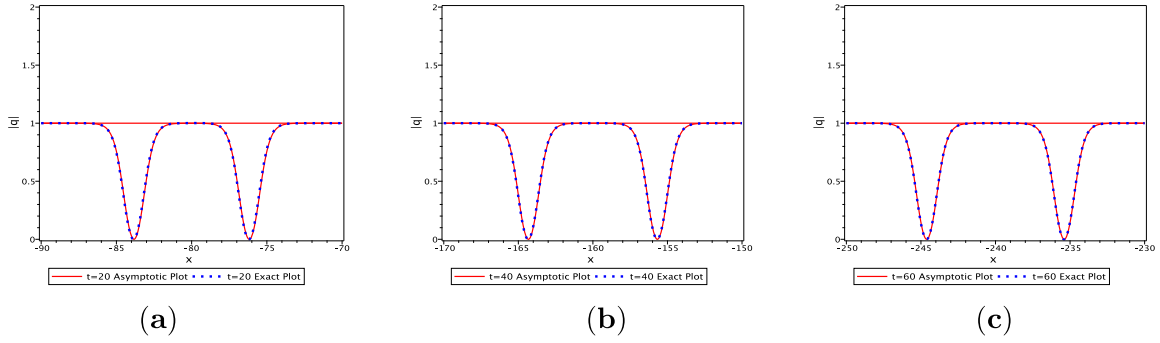

Fig. 10. The comparison between the exact solution and the asymptotic solution at time $t = 20, t = 40, t = 60$.

We would apply PINN scheme to investigate the data-driven soliton solutions of Eq. (5.1) with $\delta = 0.01, \beta = 1$. The soliton solutions include the dark soliton solution and dark–anti-dark pair solution. These solutions have be derived in Section 3, and their corresponding dynamic behavior also have been discussed above. As presented in (3.29), the precise form of these solutions can be written as follows:

Using the same parameters as Fig. 2, the exact dark soliton solution admits

$$q(x,t) = \frac{-2\sqrt{2}ie^{\sqrt{2}(4t+x)}\sin(\frac{t}{50}) - e^{2\sqrt{2}(4t+x)} + 1}{2\sqrt{2}ie^{\sqrt{2}(4t+x)}\cos(\frac{t}{50}) - e^{2\sqrt{2}(4t+x)} + 1}. \tag{5.2}$$

Using the same parameters as Fig. 4, the exact dark–anti-dark pair solution admits

$$q(x,t) = \frac{\sqrt{2}e^{4\sqrt{2}t+\sqrt{2}x-\frac{it}{50}} - 100\sqrt{2}e^{4\sqrt{2}t+\sqrt{2}x+\frac{it}{50}} - 10e^{2\sqrt{2}(4t+x)} + 10}{\sqrt{2}ie^{4\sqrt{2}t+\sqrt{2}x-\frac{it}{50}} + 100\sqrt{2}ie^{4\sqrt{2}t+\sqrt{2}x+\frac{it}{50}} - 10e^{2\sqrt{2}(4t+x)} + 10}. \tag{5.3}$$

5.1. The PINN algorithm

In this subsection, we commit to introduce the PINN algorithm [28] for the data-driven solutions in detail. The main idea of the PINN algorithm is to use a deep NN to find the solutions of Eq. (5.1). Let $q(x,t) = u(x,t) + iv(x,t)$, $q^*(-x,-t) = u(-x,-t) - iv(-x,-t)$ being its real and imaginary parts, respectively, and then substituting them into Eq. (5.1), we have

$$\begin{cases} u_t + \beta u_{xxx} + \delta u_{xx} - 6\beta[uu(-x,-t) + vv(-x,-t)]u_x \\ -2\delta u^2 u(-x,-t) \\ -6\beta[uv(-x,-t) - vu(-x,-t)]v_x + 2\delta[1 - 2vv(-x,-t)]u \\ +2\delta v^2 u(-x,-t) = 0, \\ v_t + \beta v_{xxx} + \delta v_{xx} + 6\beta[uv(-x,-t) - vu(-x,-t)]u_x \\ -2\delta v^2 v(-x,-t) \\ -6\beta[uu(-x,-t) + vv(-x,-t)]v_x \\ +2\delta[1 - 2uu(-x,-t)]v + 2\delta u^2 v(-x,-t) = 0. \end{cases} \tag{5.4}$$

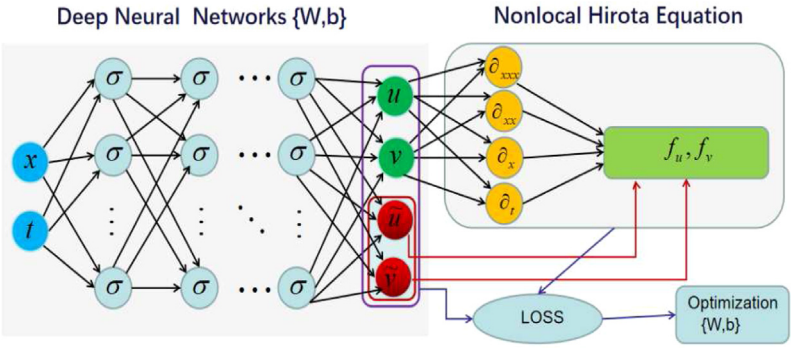

Fig. 11. The PINN scheme solving the nonlocal Hirota equation, $\tilde{u} = u(-x,-t)$, $\tilde{v} = v(-x,-t)$.

Then the physics-informed NNs $f_u(x,t), f_v(x,t)$ can be defined as

$$\begin{cases} f_u := u_t + \beta u_{xxx} + \delta u_{xx} - 6\beta[uu(-x,-t) + vv(-x,-t)]u_x \\ -2\delta u^2 u(-x,-t) \\ -6\beta[uv(-x,-t) - vu(-x,-t)]v_x + 2\delta[1 - 2vv(-x,-t)]u \\ +2\delta v^2 u(-x,-t), \\ f_v := v_t + \beta v_{xxx} + \delta v_{xx} + 6\beta[uv(-x,-t) - vu(-x,-t)]u_x \\ -2\delta v^2 v(-x,-t) \\ -6\beta[uu(-x,-t) + vv(-x,-t)]v_x + 2\delta[1 - 2uu(-x,-t)]v \\ +2\delta u^2 v(-x,-t), \end{cases} \tag{5.5}$$

of which $u(x,t;w,b)$, $v(x,t;w,b)$ represent the output of the neural network, which is an approximation of the solution $q(x,t)$. Applying automatic differentiation mechanism in $u(x,t;w,b)$, $v(x,t;w,b)$, the residual PINN $f_u(x,t), f_v(x,t)$ are given [62]. Then, the multi-hidden-layer deep NN is used to train the network parameters w, b. To obtain the optimum training results, we construct the following Loss functions which can be minimized via using L-BFGS optimization method [63]

$$Loss_\Theta = Loss_u + Loss_v + Loss_{f_u} + Loss_{f_v}, \tag{5.6}$$

with

$$\begin{cases} Loss_u = \frac{1}{N_q}\sum_{i=1}^{N_q} |\hat{u}(x_q^i, t_q^i) - u^i|^2, \\ Loss_v = \frac{1}{N_q}\sum_{i=1}^{N_q} |\hat{v}(x_q^i, t_q^i) - v^i|^2, \\ Loss_{f_u} = \frac{1}{N_f}\sum_{l=1}^{N_f} |f_u(x_f^l, t_f^l)|^2, \\ Loss_{f_v} = \frac{1}{N_f}\sum_{l=1}^{N_f} |f_v(x_f^l, t_f^l)|^2, \end{cases} \tag{5.7}$$

where $\{x_q^i, t_q^i, u^i\}_{i=1}^{N_q}$ and $\{x_q^i, t_q^i, v^i\}_{i=1}^{N_q}$ denote the sampling initial and boundary value training data, respectively. $\{x_f^l, t_f^l\}_{l=1}^{N_f}$ denote the sampling collocation points for f_u and f_v. On the one hand, the loss function (5.6) makes the learning solution approximate the exact one, on the other hand, it makes the hidden $\hat{u}$, $\hat{v}$ satisfy the target nonlinear partial differential Eq. (5.1). To understand PINN algorithm more intuitively, the flow chart of PINN algorithm for nonlocal Hirota equation is shown in Fig. 11, in which NN and physical information part can be seen. The aim is to optimize the loss function using the NN part as well as the physics information part.

To obtain the data-driven soliton solution for the nonlocal Hirota equation (5.1), we choose the PINN which contains 9-hidden-layer NN with each layer having 40 neurons. Their activation functions both are the hyperbolic tangent (tanh). The all codes are written by Python 3.7 and run on Tensorflow 1.15, and the corresponding hardware is a HP Laptop 14s-dr2xxx with 2.40 GHz 4-core 11th Gen Intel Core i5-1135G7 and 16 GB memory.

5.2. The data-driven dark soliton solution

First, we take $[x_0, x_1] = [-3, 3]$ and $[t_0, t_1] = [-3, 3]$ in Eq. (5.1) as the boundary conditions, and select the following initial condition arising from the dark soliton solution (5.2)

$$q_0(x) = q(x, -3), \tag{5.8}$$

and the Dirichlet boundary conditions for Eq. (5.1)

$$q_{lb}(t) = q(-3, t),\ q_{ub}(t) = q(3, t),\ t \in [-3, 3]. \tag{5.9}$$

In terms of MATLAB software, the traditional finite difference method can be used to capture the original training data by dispersing Eq. (5.2) with dividing spatial region $[-3, 3]$ into 1500 points and time region $[-3, 3]$ into 1000 points. The original training data contains the initial boundary data and the inner points. Here, we choose $N_q = 1500$ as the random sample points from initial boundary data and $N_f = 30000$ as random collocation points from the inner points based on the Latin hypercube sampling (LHS) method [64]. Processing these obtained training data in the PINN scheme, the data-driven dark soliton solution $q(x,t)$ can be eventually learned, which has a 2.695814e−04 $\mathbb{L}_2$-norm error compared with the exact one. The total learning process executes 927 times and takes about 1262.4172 s. The corresponding dynamic behaviors are displayed in the following Figs. 12 and 13.

In Fig. 12, the wave propagation pattern along the x-axis and the density plots for the data-driven dark soliton solution are shown respectively. From Fig. 12, it is easy to find that the error range is about −0.001 to 0.001 between the learned dynamics and error dynamics. This fact can verify that the simulation is pretty good. Fig. 13 is the three-dimensional plot and loss curve figure of data-driven dark soliton solution.

5.3. The data-driven dark–anti-dark pair solution

For data-driven periodic wave solution, we let $[x_0, x_1] = [-5, 5]$ and $[t_0, t_1] = [-5, 5]$ in Eq. (5.1) as the boundary conditions, and select the following initial condition arising from the dark–anti-dark pair solution(5.3)

$$q_0(x) = q(x, -5), \tag{5.10}$$

and the Dirichlet boundary conditions

$$q_{lb}(t) = q(-5, t),\ q_{ub}(t) = q(5, t),\ t \in [-5, 5]. \tag{5.11}$$

Carrying out the same process as Section 4.2, the data-driven dark–anti-dark pair solution is generated successfully. The results of the experiment show that the $\mathbb{L}_2$-norm error between learning

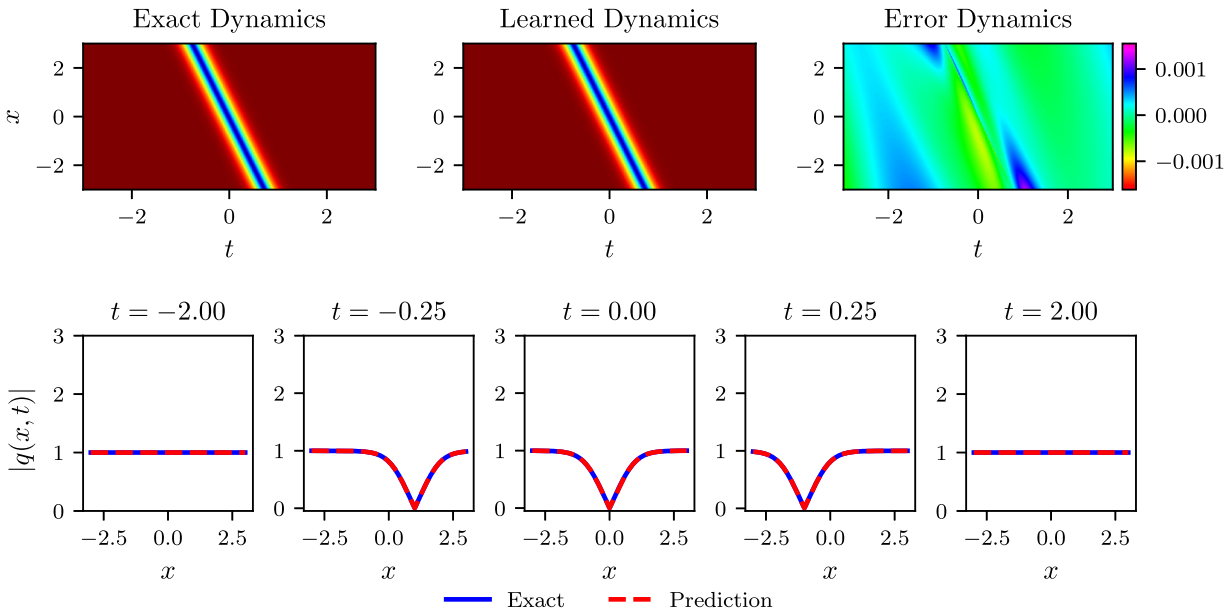

Fig. 12. The data-driven dark soliton solution $q(x,t)$ for nonlocal Hirota equation (5.1): The exact, learned and error dynamics density plots, and the sectional drawings which contain the learned and explicit dark soliton solution $q(x,t)$ at the five distinct times $t=-2, t=-0.25, t=0, t=0.25, t=2$.

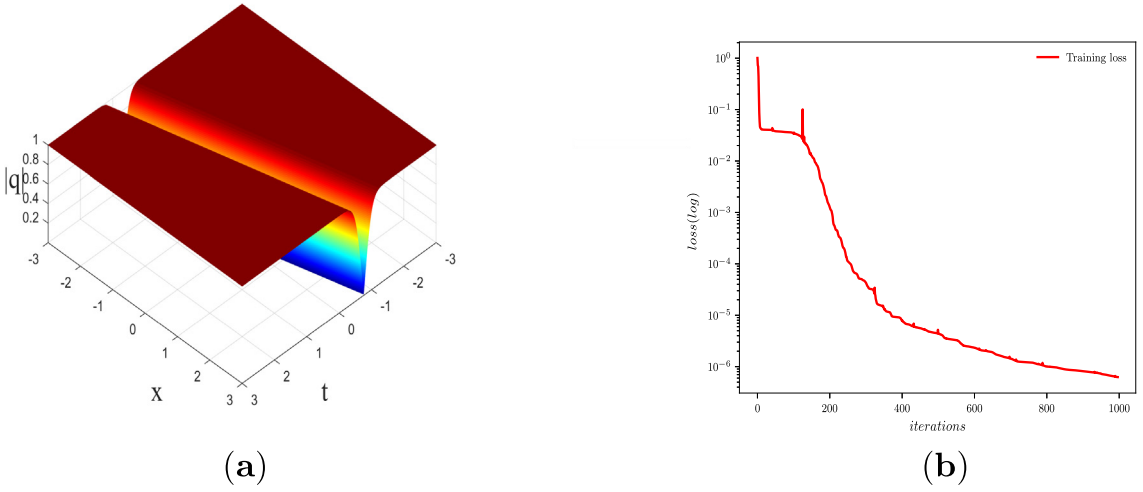

Fig. 13. The data-driven dark soliton solution $q(x,t)$ for nonlocal Hirota equation (5.1): (**a**) The three-dimensional plot; (**b**) The loss curve figure.

solution $q(x,t)$ and exact one is 8.243617e−04, and the whole learning process iterates 1807 times with costing 2737.0690 s. The main dynamic behaviors for the data-driven dark–anti-dark pair solution are plotted in Figs. 14 and 15. From these plots, we also find the learning effect is pretty good with a very small error and a rapidly decaying Loss curve.

5.4. The PINN algorithm for the data-driven parameter discovery

In this section, we put our attention to the problem of data-driven discovery of nonlocal Hirota equation (5.1) by using PINN algorithm. Our goal is to identify the parameters δ, β in terms of the dark soliton solution (5.2). In the same way, the physics-informed neural networks $f_u(x,t), f_v(x,t)$ for Eq. (5.1) are given in (5.5).

Using the Latin Hypercube Sampling, a training data set can be generated through selecting randomly $N_q = 1500$ as the initial boundary data and $N_f = 30000$ as the collocation points with the aid of the exact soliton solution (5.2) with $\delta = 0.01, \beta = 1$ and $(x,t) \in [-3,3] \times [-3,3]$. In terms of the obtained training data set, using a 9-hidden-layer deep PINN with 40 neurons per layer, the data-driven parameters δ, β can be discovered. The corresponding results are summarized in Table 1. We observe that the PINN is able to correctly identify the unknown parameters with very high accuracy when the training data was corrupted without noise. Specifically, as we can see in Table 1, at the case of 0.005 noise and 0.01 noise, the error of parameters δ and β is still receivable, which illustrates that the predictions remain robust. Of course, we can also find that noise has a bad effect on the error value of parameters.

The variation of unknown parameters and loss functions with iteration is analyzed when different noises are used in inverse problems. Fig. 16(a) and (b) show the changes of unknown parameters with iteration under different noises. We find that the unknown parameters fluctuate less in the absence of noise, but the parameters fluctuate more as the noise increases. Fig. 16(c)

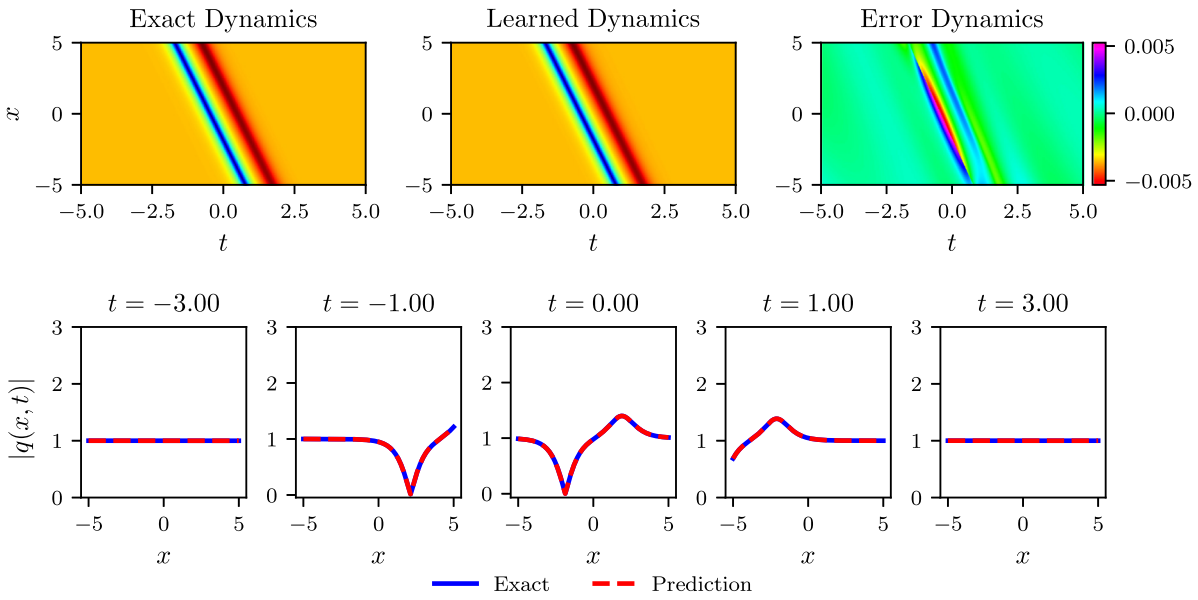

Fig. 14. The data-driven dark–anti-dark pair solution $q(x,t)$ for nonlocal Hirota equation (5.1): The exact, learned and error dynamics density plots, and the sectional drawings which contain the learned and explicit dark–anti-dark pair solution $q(x,t)$ at the five distinct times $t=-3, t=-1, t=0, t=1, t=3$.

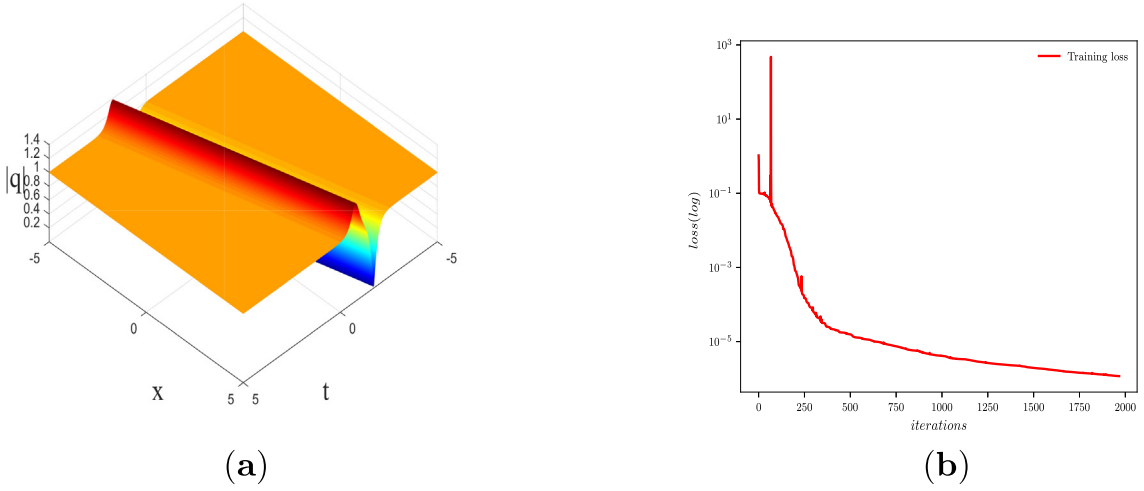

Fig. 15. The data-driven dark–anti-dark pair solution $q(x,t)$ for nonlocal Hirota equation (5.1): (**a**) The three-dimensional plot; (**b**) The loss curve figure.

Table 1
Data-driven parameter discovery of δ, β in the sense of dark soliton.

Noise	Parameter			
	δ	error of δ	β	error of β
Correct parameter	0.01	0	1	0
Without noise	0.00976523	2.34770×10^{-2}	0.9998441	1.559×10^{-4}
With a 0.005 noise	0.01055261	5.52606×10^{-2}	0.9998072	1.928×10^{-4}
With a 0.01 noise	0.00934824	6.51762×10^{-2}	0.9998599	1.401×10^{-4}

depicts the changes of loss functions for different noises as the number of iterations increases. It indicates that the convergence effect becomes worse and worse with the increase of noise. Therefore, we can conclude that when discovering the physical parameters of the model, the less noise the better the training effect.

6. Conclusions and discussions

In this paper, we have applied the RH method to discuss the nonlocal Hirota equation with NZBCs. Through solving the RH problem at the case of simplify poles, we have given out the general N-soliton solutions for the nonlocal Hirota equation under NZBCs. The critical technique shown in this work is to eliminate the properties of singularities via subtracting the residue from the original non-regular RH problem when reflection coefficients have simplify poles. For the case of double poles, we also need to subtract the extra coefficient L_2. Additionally, the asymptotic value of jump matrix is subtracted from the original non-regular RH problem. Then the regular RH problem can be displayed, which can be solved by Plemelj formula. Finally, the N-simplify poles and N-double poles solutions can be derived by using the

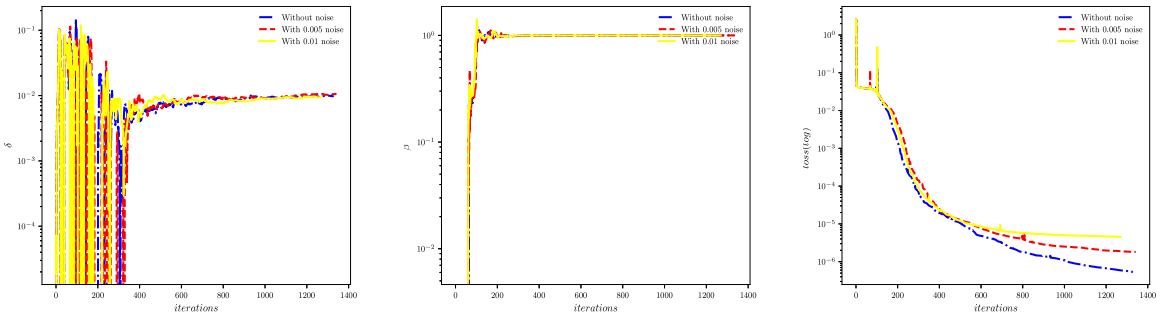

Fig. 16. (**a**, **b**) The variation of unknown parameters δ, β and (**c**) the variation of loss function with the different noise.

solution of RH problem to reconstruct potential function. Compared with the local Hirota equation, the symmetry reductions of Just solutions and scattering matrix are different, which results in a disparate discrete spectra distribution. The dynamical patterns of one-simplify pole solution with different parameters and one-double pole solution have been discussed in detail. Especially, some novel dynamic behaviors have been found for the nonlocal Hirota equation and the asymptotic state of one-double poles solution was discussed. Furthermore, we will study the long time asymptotic behaviors for the nonlocal Hirota equation with NZBCs via the Deift–Zhou method in another paper.

Additionally, we have also studied the data-driven soliton solutions and parameters discovery for the nonlocal Hirota equation with Dirichlet boundary conditions via the PINN method. Remarkably, due to the nonlocal Hirota equation has $\mathcal{PT}$ symmetry term, it is quite different with the local Hirota equation. Through adding the nonlocal term into the NN, we can successfully handle the $\mathcal{PT}$ symmetry term and give out the data-driven soliton solutions and the parameter prediction for the nonlocal Hirota equation. Our results indicate that the deep learning can be applied to solve nonlocal integrable systems.

CRediT authorship contribution statement

Wei-Qi Peng: Writing – original draft, Writing – review & editing, Conceptualization, Formal analysis, Software. **Yong Chen:** Writing – review & editing, Supervision, Project administration.

Declaration of competing interest

The authors declare that they have no known competing financial interests or personal relationships that could have appeared to influence the work reported in this paper.

Acknowledgments

This work was supported by the project is supported by National Natural Science Foundation of China (No. 12175069) and Science and Technology Commission of Shanghai Municipality, China (No. 21JC1402500 and No. 18dz2271000).

References

[1] M.J. Ablowitz, P.A. Clarkson, Solitons; Nonlinear Evolution Equations and Inverse Scattering, Cambridge University Press, Cambridge, 1991.
[2] R. Hirota, Direct Methods in Soliton Theory, Springer, Berlin, 2004.
[3] V.B. Matveev, M.A. Salle, Darboux Transformation and Solitons, Springer, Berlin, 1991.
[4] C.S. Gardner, J.M. Greene, M.D. Kruskal, R.M. Miura, Method for solving the KortewegdeVries equation, Phys. Rev. Lett. 19 (1967) 1095.
[5] V.E. Zakharov, S.V. Manakov, S.P. Novikov, L.P. Pitaevskii, The Theory of Solitons: The Inverse Scattering Method, Consultants Bureau, New York, 1984.
[6] J. Yang, Nonlinear waves in integrable and non-integrable systems, Soc. Ind. Appl. Math. (2010).
[7] Y. Li, S.F. Tian, J.J. Yang, Riemann-Hilbert problem and interactions of solitons in the n-component nonlinear Schrödinger equations, Stud. Appl. Math. (2021).
[8] B.L. Guo, L.M. Ling, Riemann-Hilbert approach and N-soliton formula for coupled derivative Schrödinger equation, J. Math. Phys. 53 (2012) 133–3966.
[9] W.Q. Peng, S.F. Tian, X.B. Wang, et al., Riemann-Hilbert method and multi-soliton solutions for three-component coupled nonlinear Schrödinger equations, J. Geom. Phys. 146 (2019) 103508.
[10] B. Yang, Y. Chen, High-order soliton matrices for Sasa-Satsuma equation via local Riemann-Hilbert problem, Nonlinear Anal. RWA 45 (2019) 918–941.
[11] X.G. Geng, J.P. Wu, Riemann-Hilbert approach and N-soliton solutions for a generalized Sasa-Satsuma equation, Wave Motion. 60 (2016) 62–72.
[12] Y.S. Zhang, J.G. Rao, Y. Cheng, J.S. He, Riemann-Hilbert method for the Wadati-Konno-Ichikawa equation N simple poles and one higher-order pole, Physica D 399 (2019) 173–185.
[13] D.S. Wang, D.J. Zhang, J. Yang, Integrable properties of the general coupled nonlinear Schrödinger equations, J. Math. Phys. 51 (2010) 023510.
[14] G. Biondini, G. Kovačič, Inverse scattering transform for the focusing nonlinear Schrödinger equation with nonzero boundary conditions, J. Math. Phys. 55 (2014) 031506.
[15] G. Biondini, E. Fagerstrom, B. Prinari, Inverse scattering transform for the defocusing nonlinear Schrödinger equation with fully asymmetric non-zero boundary conditions, Physica D 333 (2016) 117–136.
[16] G.Q. Zhang, Z.Y. Yan, Inverse scattering transforms and soliton solutions of focusing and defocusing nonlocal mKdV equations with non-zero boundary conditions, Physica D. 402 (2019) 132170.
[17] N. Liu, B. Guo, Solitons and rogue waves of the quartic nonlinear Schrödinger equation by Riemann-Hilbert approach, Nonlinear. Dyn. 100 (2020) 629–646.
[18] Z.C. Zhang, E.G. Fan, Inverse scattering transform for the Gerdjikov-Ivanov equation with nonzero boundary conditions, Z. Angew. Math. Phys. (2020) 71.
[19] D. Bilman, P.D. Miller, A robust inverse scattering transform for the focusing nonlinear Schrödinger equation, Comm. Pure Appl. Math. 72 (8) (2019) 1722–1805.
[20] S.Y. Chen, Z.Y. Yan, The higher-order nonlinear Schrödinger equation with non-zero boundary conditions: robust inverse scattering transform, breathers, and rogons, Phys. Lett. A. 383 (29) (2019) 125906.
[21] X.E. Zhang, Y. Chen, Inverse scattering transformation for generalized nonlinear Schrödinger equation, Appl. Math. Lett. 98 (2019) 306–313.
[22] Y.S. Zhang, X.X. Tao, T.T. Yao, J.S. He, The regularity of the multiple higher-order poles solitons of the NLS equation, Stud. Appl. Math. 145 (4) (2020) 812–827.
[23] J.J. Yang, S.F. Tian, Z.Q. Li, Riemann-Hilbert problem for the focusing nonlinear Schrödinger equation with multiple high-order poles under nonzero boundary conditions, Physica D 432 (2022) 133162.
[24] Z.Y. Wang, S.F. Tian, J. Cheng, The Dbar-dressing method and soliton solutions for the three-component coupled Hirota equations, J. Math. Phys. 62 (2021) 093510.
[25] S.F. Tian, Riemann-Hilbert problem to a generalized derivative nonlinear Schrödinger equation: Long-time asymptotic behavior, Sci. Sin Math. 51 (2021) 1–38.
[26] L.M. Ling, X.E. Zhang, Large and infinite order solitons of the coupled nonlinear Schrödinger equation, 2021, arXiv preprint arXiv:2103.15373.

[27] D. Bilman, L.M. Ling, P.D. Miller, Extreme superposition: Rogue waves of infinite order and the painlev-III hierarchy, Duke Math. J. 169 (4) (2020) 671–760.
[28] M. Raissi, P. Perdikaris, G.E. Karniadakis, Physics-informed neural networks: A deep learning framework for solving forward and inverse problems involving nonlinear partial differential equations, J. Comput. Phys. 378 (2019) 686–707.
[29] J. Li, Y. Chen, Solving second-order nonlinear evolution partial differential equations using deep learning, Commun. Theor. Phys. 72 (2020) 105005.
[30] J.C. Pu, J. Li, Y. Chen, Solving localized wave solutions of the derivative nonlinear Schrödinger equation using an improved PINN method, Nonlinear Dynam. 105 (2) (2021) 1–17.
[31] W.Q. Peng, J.C. Pu, Y. Chen, PINN deep learning for the chen-lee-liu equation: rogue wave on the periodic background, Commun. Nonlinear Sci. Numer. Simul. 105 (2022) 106067.
[32] S.N. Lin, Y. Chen, A two-stage physics-informed neural network method based on conserved quantities and applications in localized wave solutions, J. Comput. Phys. (2022) 111053.
[33] L. Wang, Z.Y. Yan, Data-driven rogue waves and parameter discovery in the defocusing nonlinear Schrödinger equation with a potential using the PINN deep learning, Phys. Lett. A (2021) 127408.
[34] Y. Fang, G.Z. Wu, Y.Y. Wang, C.Q. Dai, Data-driven femtosecond optical soliton excitations and parameters discovery of the high-order NLSE using the PINN, Nonlinear Dynam. (2021) 1–14.
[35] R.Q. Wang, L.M. Ling, D.L. Zeng, B.F. Feng, A deep learning improved numerical method for the simulation of rogue waves of nonlinear Schrödinger equation, Commun. Nonlinear Sci. Numer. Simul. 101 (2021) 105896.
[36] Y.F. Mo, L.M. Ling, D.L. Zeng, Data-driven vector soliton solutions of coupled nonlinear Schrödinger equation using a deep learning algorithm, Phys. Lett. A (2021) 127739.
[37] R. El-Ganainy, K. Makris, D. Christodoulides, Z.H. Musslimani, Theory of coupled optical $\mathcal{PT}$-symmetric structures, Opt. Lett. 32 (2007) 2632.
[38] C.M. Bender, B.K. Berntson, D. Parker, E. Parker, Observation of PT phase transition in a simple mechanical system, Amer. J. Phys. 81 (2013) 173.
[39] T. Gadzhimuradov, A. Agalarov, Towards a gauge-equivalent magnetic structure of the nonlocal nonlinear Schrödinger equation, Phys. Rev. A. 93 (2016) 62124.
[40] C.M. Bender, S. Boettcher, H.F. Jones, P.N. Meisinger, M. Simsek, Bound states of non-Hermitian quantum field theories, Phys. Lett. A. 71 (2003) 1095.
[41] B. Bagchi, C. Quesne, Sl(2, C) as a complex Lie algebra and the associated non-hermitian Hamiltonians with real eigenvalues, Phys. Lett. A. 273 (2000) 285.
[42] D. Mihalache, Multidimensional localized structures in optical and matter-wave media: a topical survey of recent literature, Rom. Rep. Phys. 69 (2017) 403.
[43] M.J. Ablowitz, Z.H. Musslimani, Integrable nonlocal nonlinear Schrödinger equation, Phys. Rev. Lett. 110 (2013) 64105.
[44] A.S. Fokas, Integrable multidimensional versions of the nonlocal nonlinear Schrödinger equation, Nonlinearity 29 (2016) 319.
[45] J.G. Rao, Y. Cheng, J.S. He, Rational and semi-rational solutions of the nonlocal Davey–Stewartson equations, Stud. Appl. Math. 139 (2017) 568.
[46] Z.X. Zhou, Darboux transformations and global explicit solutions for nonlocal Davey–Stewartson I equation, Stud. Appl. Math. 141 (2018) 186.
[47] M.M. Wang, Y. Chen, Dynamic behaviors of general N-solitons for the nonlocal generalized nonlinear Schrödinger equation, Nonlinear Dynam. 104 (2021) 2621–2638.
[48] H.J. Zhou, Y. Chen, Breathers and rogue waves on the double-periodic background for the reverse-space–time derivative nonlinear Schrödinger equation, Nonlinear Dynam. (2021).
[49] M.J. Ablowitz, Z.H. Musslimani, Inverse scattering transform for the integrable nonlocal nonlinear Schrödinger equation, Nonlinearity 29 (2016) 915–946.
[50] M.J. Ablowitz, Z.H. Musslimani, Integrable nonlocal nonlinear equations, Stud. Appl. Math. 139 (2017) 7–59.
[51] J.L. Ji, Z.N. Zhu, Soliton solutions of an integrable nonlocal modified Korteweg–de Vries equation through inverse scattering transform, J. Math. Anal. Appl. 453 (2017) 973–984.
[52] M.J. Ablowitz, X.D. Luo, Z.H. Musslimani, Inverse scattering transform for the nonlocal nonlinear Schrödinger equation with nonzero boundary conditions, J. Math. Phys. 59 (2018) 011501.
[53] M.J. Ablowitz, B.F. Feng, X.D. Luo, Z.H. Musslimani, Reverse space–time nonlocal sine-gordon/sinh-gordon equations with nonzero boundary conditions, Stud. Appl. Math. 141 (2018) 267–307.
[54] M.J. Ablowitz, B.F. Feng, X.D. Luo, Z.H. Musslimani, Inverse scattering transform for the nonlocal reverse space-time nonlinear Schrödinger equation, Theoret. Math. Phys. 196 (3) (2018) 1241–1267.
[55] B.F. Feng, X.D. Luo, M.J. Ablowitz, Z.H. Musslimani, General soliton solution to a nonlocal nonlinear Schrödinger equation with zero and nonzero boundary conditions, Nonlinearity 31 (12) (2018) 5385.
[56] G.Q. Zhang, Z.Y. Yan, Inverse scattering transforms and soliton solutions of focusing and defocusing nonlocal mKdV equations with nonzero boundary conditions, Physica D 402 (2020) 132170.
[57] X.F. Zhang, S.F. Tian, J.J. Yang, Inverse scattering transform and multiple high-order pole solutions for the nonlocal focusing and defocusing modified Korteweg–de Vries equation with the nonzero boundary conditions, 2021, arXiv preprint arXiv:2109.02901.
[58] J. Cen, C. Francisco, F. Andreas, Integrable nonlocal Hirota equations, J. Math. Phys. 60 (8) (2019) 081508.
[59] Y. Li, S.F. Tian, Inverse scattering transform and soliton solutions of an integrable nonlocal Hirota equation, Commun. Pure Appl. Anal. (2021).
[60] Y.R. Xia, R.X. Yao, X.P. Xin, Darboux transformation and soliton solutions of a nonlocal Hirota equation, Chin. Phys. B (2021).
[61] N.N. Li, R. Guo, Nonlocal continuous Hirota equation: Darboux transformation and symmetry broken and unbroken soliton solutions, Nonlinear Dyn. 105 (2021) 617–628.
[62] A.G. Baydin, B.A. Pearlmutter, A.A. Radul, J.M. Siskind, Automatic differentiation in machine learning: a survey, J. Mach. Learn. Res. 18 (2018) 1–43.
[63] D.C. Liu, J. Nocedal, On the limited memory BFGS method for large scale optimization, Math. Program 45 (1989) 503–528.
[64] M. Stein, Large sample properties of simulations using Latin hypercube sampling, Technometrics 29 (1987) 143–151.